CONTROL OF MICROMANIPULATION IN THE PRESENCE OF VAN DER WAALS FORCE

CHUA, KIAN TI

(*B. Eng.(Hons.), The University of Adelaide*)

A THESIS SUBMITTED

FOR THE DEGREE OF MASTER OF ENGINEERING

DEPARTMENT OF MECHANICAL ENGINEERING

NATIONAL UNIVERSITY OF SINGAPORE

2003

Acknowledgement

My first gratitude goes to Dr. Peter Chen for his many suggestions and constant support during this research. Without his effort, this thesis would not have been possible.

I would like to express my sincere gratitude to Prof. Poo Aun Neow for his guidance and support as well as the opportunity provided to me as a research student.

I would also like to thank Dr. Cheryl Li for her guidance and advices through the early time of chaos and confusion.

Finally, many thanks to my friends Hock Chan, Horng Yih, Sheau Chin, Chee Kiong and others for their support and helpful comments.

Table of Contents

Summary

Micromanipulation plays an important role in the industrial and academic areas. For instance, it is used in the surgery and manufacturing of micro-parts. The wide applications make it an active research area. Since motion is much smaller than in conventional manipulation systems, the existing technology has to be reviewed. It is known that microscopic forces, like van der Waals and electrostatic forces, become significant in the micro-systems. The gravitational force is, however, insignificant and can be ignored. One of the problems caused by the microscopic forces, which never considered in the conventional system, is the adhesive effect which the objects are adhered to the tool resulting in problems in picking and releasing. Another problem arising is the long-range effect of microscopic forces such as the van der Waals force. The significant amount of the van der Waals force can disturb the dynamics of the system. The control of the micromanipulation system has to be able to attenuate the effect of van der Waals forces. The first problem has been studied in much literature and is not considered in this thesis. On the other hand, the second problem is also worth the study since the understanding of the van der Waals force effect on the system may help to improve the performance of micromanipulation. We decided to make it the centre of this thesis.

The main purpose of the thesis is to investigate various control approaches

on a micromanipulation system under the influence of van der Waals force. It also examines the ability of the control laws in attenuating the effect of van der Waals force on the system. The control laws covered includes both linear and nonlinear. A general conceptual micromanipulation system was developed for the investigation. The system consists of a piezostack actuator, a gripping tool and spheres. The objective is to move an object from a distance to 'touch' another object. During this motion, the system exhibits significant van der Waals force. A dynamic model of the system was developed. It includes the van der Waals force between two spheres. System parameters and a desired trajectory were also determined for simulations. The linear controllers employed are the PID and lead-lag control, which are both simple and easy to implement. The nonlinear control law applied is the inverse dynamics robust control, which uses a technique so-called Second method of Lyapunov. This robotic control law uses the desired trajectory to calculate the required torque 'inversely' which is able to give low position error. Robustness of the control is achieved by adding the extra control signal. This additional control is derived from the estimation of bound system uncertainty or modelling error. In the derivation of control law, van der Waals force is treated as the system uncertainty for the estimation. The Lyapunov equation is also used in the derivation which ensures the stability. This nonlinear control is found to give very low position tracking error. Its robustness is able to reduce the effect of van der Waals force on the system.

Nomenclature

A	Hamaker constant (J)
$A, \bar{A}, B$	state space matrix parameters
B	electric field strength (V/mm)
C	distance between centers of spheres (m);
	controller equation or transfer function;
	coriolis and centrifugal force vector
D	initial height of sphere A (m)
E	Young's Modulus (Pa); system uncertainty parameters; error
F	force (N)
F_p	force exerted by piezostack (N)
F_{vdW}, F_v, F_h	van der Waals force (N)
G	plant transfer function
H	system parameter consists of coriolis and centrifugal, frictional
	and gravitational force.
$\hat{H}, \hat{M}$	incorrectly-modelled system parameters
$\Delta H, \Delta M$	modelling error of system parameters
I	identity matrix
K	controller gain
K_1, K_2	position and velocity gain matrix

K_P	proportional control gain
K_I	integral control gain
K_D	derivative control gain
L	length of piezostack (m)
M	mass (kg); inertia matrix
N	number of piezodiscs in piezostack
P, Q	positive define matrices in Lyapunov equation
$\bar{Q}, \alpha, \phi, \overline{M}$	bounds of system parameters
R	radius of sphere (m); reference input
T	closed-loop transfer function
W	interaction energy (J)
V	voltage (V)
Y	system output
c	damping coefficient (Ns/m)
d_{33}	piezoeletric charge constant (m/V)
e	error
f	function
g	gravitational force (N)
h	Planck's constant (6.626×10^{-34} Js)
k	stiffness (N/m)
k_p	stiffness of piezostack (m)
l	horizontal distance between centers of spheres A and B (m)
m	mass (kg)
m_p	mass of piezostack (kg)
m_s	mass of sphere (kg)
p	pole in lead-lag compensator

q	number of atoms or molecules per unit volume (m^{-3}),
	vector of joint variables, position vector
q^d, x_d	desired position
r	distance between two atoms or molecules (m);
	reference input vector
r_p	radius of piezostack (m)
s	variable in transfer function
t	time (sec)
u	control signal
v	orbiting frequency of the electron (Hz); feedback control input
Δv	additional feedback control input
w_i	natural frequency
x	position (m)
x_v	displacement due to van der Waals force
z	zero in lead-lag compensator
α_0	electronic polarizability ($C^2m^2J^{-1}$)
δ	nearest surface separation of two spheres (m)
ε_0	permittivity of free space (8.854×10^{-12} $C^2m^{-1}J^{-1}$)
η	uncertainty
θ	angle (deg or rad)
λ	London-van der Waals constant (Jm^6)
ρ	continuous function for Δv estimation; density
ω_{pd}	pole added to derivative path in PID control

List of Figures

List of Tables

Chapter 1

Introduction

In these last few years, robotics has entered a new era since micro-technology was introduced. Micro-robotics became a popular and active research area, and micro-manipulation has become particular interest due to its wide applications such as in the manufacture of micro-parts, micro-machines and devices. Applications have extended to microsurgery and other bioengineering related areas. One example is the molecular surgery of DNA by Yamamoto [1]. However micromanipulation requires different principles and implementation than usual macro-manipulation. Many new aspects to be taken care of.

1.1 Problems in Micromanipulation

Micromanipulation deals with the manoeuvre of tiny objects such as human cells. The environment and the mechanics of the system are different from classical prehension. It is expected that classical knowledge, including control and modelling, may not be applied fully. In addition, conventional devices may not be able to handle the micro-scale motion. For example, it is not possible to use normal force sensors down to nanonewtons. These differences between micro and macro-manipulation require research and development in the theoretical and practical aspects of micromanipulation.

Generally, the weight of the objects being manipulated is ignored in microscopic sizes as its effect is relatively insignificant. For instance, in this thesis, the weight of the sphere being manipulated is at the order of 10^{-11}N while the van der Waals force is at the order of 10^{-7}N (see Chapter 4). On the other hand, other microscopic forces, such as van der Waals force, which are not normally considered in macro-scale systems become significant. Beside van der Waals force, electrostatic force and surface tension are also significant in the microscopic world. However, they can be reduced to a very small amount. Papers [2]-[3] described that the capillary force is very much dependent on the humidity. They suggested that setting low humidity condition and applying hydrophobic treatment to the object surface can greatly reduce the capillary force. Electrostatic force arises when charges are generated on the micro-objects. Sitti et. al.[4] suggested that if the objects are coated with gold and by grounding all the substrate and objects, the electrostatic forces can be negligible. Arai et. al.[2] and Feddema et. al.[5] studied their micromanipulation subject while neglecting the capillary and electrostatic forces and only focused on the van der Waals force. Based on the study above, the author ignored the effect of capillary and electrostatic force while only focused van der Waals force in the thesis.

One of the major influence of the microscopic forces is the sticking between objects. This affects the motion of picking up and releasing of tiny objects. There are a lot of literature studying this problem. For example, Arai et. al.[6] constructed a gripper with 'Micropyramid' on contact surface to reduce the contact adhesion force. Similar concept was also used by Zhou et. al.[7] who increased the roughness of gripper finger surface to achieve lower contact adhesion force. Rollot et. al.[8] developed an object releasing model and a set of release condition including material combinations, geometry and speed. He concluded

that at certain combinations, the successful releasing rate of micro-object was higher. Feddema et. al.[5] studied the contact adhesion forces and motion planning on pick and release of a spherical particle. More studies can be found in [2], [3] and [4]. Since the contact force appears to be well studied, it will not be studied in this thesis.

Another major influence of the microscopic force which is seldom seen in the literature is the long-range effect of the micro-forces. In inter-molecular terms, long-range means distance of few nano-metres which is long compared to the 'touching' distance of two particles about 0.165nm between surfaces. It is well-known that the van der Waals force is a long-range force. At a distance of few nanometers, objects can attract each other due to the inherent van der Waals force. The attraction is able to disturb the motion of the system. Unlike the capillary and electrostatic forces which can be reduced to a very low amount as mentioned above by changing the working environment parameters, the van der Waals force always exists and it is contributing a large force. Therefore, this project focuses on the long-range influence of the van der Waals force on the micromanipulation system and assumes that other microscopic forces are negligible.

1.2 Problem Formulation

The purpose of the thesis is to investigate the influence of van der Waals force on various control methods in micromanipulation, and how the van der Waals force affects the position tracking of the system and the ability of the control methods in dealing with the van der Waals force. For the investigation, a typical operation of micromanipulation – an object transferring system, will be used. The system centers on transferring one object from a starting point towards another object. The range of motion is within few nanometres. In this range, the van der Waals

force shows significant effect on the system dynamics. Thus, the effectiveness of the control methods in dealing with van der Waals force can be seen clearly.

Consider a general single degree of freedom system as shown in Figure 1.1. The object A is pushed by an actuating force F_p towards Object B. F_v is the van der Waals force acting between A and B. During the motion, while the distance between two objects is getting smaller, the van der Waals force is varying from a small amount to a large force. It is able to disturb the trajectory of the moving object. In modelling, it is treated as an additional force other than the actuating force. The dynamic equation of Object A can be expressed as

$$m\ddot{x} + c\dot{x} + kx = F_p + F_v \tag{1.1}$$

where

m = mass

c = damping coefficient

k = stiffness

x = displacement.

In micromanipulation, F_v always exists and can not be diminished. A controller is to be designed to gives accurate result while taking into account this additional force.

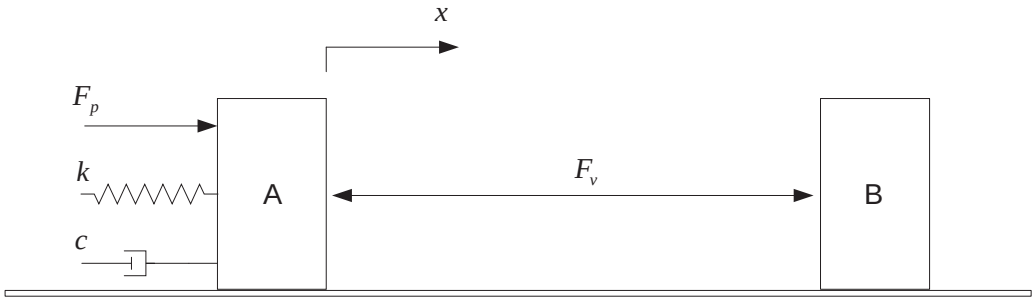

Figure 1.1: *The single degree of freedom system*

In the thesis, the system is assumed to be actuated by a piezoelectric stack. Ignoring hysteretic behaviour, the piezostack can be modelled as a general linear mass-damper-spring system. The van der Waals force is derived from the London equation for the dispersion interaction energy between two atoms or molecules. Using the additivity property, the non-retarded van der Waals force formula can be obtained. In order to run computer simulations, parameters such as system geometries, material properties and working conditions are established. Besides, a reference trajectory is also designed as a desired input for simulation to give better understanding of the van der Waals force effect.

1.3 Control and Simulations

Due to microscopic forces on the system, the control used in macroscopic system may not work properly in micromanipulation. To examine the efficiency of control methods for micromanipulation, this thesis simulates the micromanipulation task with several control methods. The micromanipulation system investigated in the thesis is a linear system, so at first glance linear control laws should be able to control it. However, the van der Waals force is complex and depends on system state. This makes the system dynamics nonlinear and may require a nonlinear control law. Hence, both linear and nonlinear controllers are investigated and compared to control the system. Linear controllers used are a conventional PID and a lead-lag compensator, which are simple and easy to implement. Integral part's ability of rejecting disturbance may also help in the control.

The nonlinear control law employed is the inverse dynamics robust control. Inverse dynamics technique is widely used in robot control. It uses the given trajectory and model of the system to calculate the torque required to perform the desired motion. The incorporated robust control method is an algorithm which

estimates the bound of system uncertainty or modelling error and determines an extra control signal to eliminate the uncertainty effect. In addition, it is required to solve the Lyapunov equation for the control signal and, hence, the stability of the system can be achieved. The method is also known as the Second Method of Lyapunov.

In this thesis, simulation are conducted to verify the analytical results. The controlled systems are simulated using MATLAB Simulink®. The results are presented by using the position tracking errors. The system simulations are conducted in two modes, with and without van der Waals force. By comparing the position tracking errors of these two modes, the ability of the control methods in attenuating the van der Waals force can be observed. Figure 1.2 shows the result of the three control methods in dealing with the van der Waals force. Smaller values indicate smaller effect of van der Waals force on the system. PID control is worse in the transient response but efficient at steady state. The curve converges at around 3.49×10^{-21}. Lead-lag compensation has a better response in transient state. However, the steady state response is the worst. The inverse dynamics robust control has excellent performance throughout the whole process. Value at steady state is around 1.33×10^{-21} which is the smallest among all. It has the best ability to attenuate the van der Waals force.

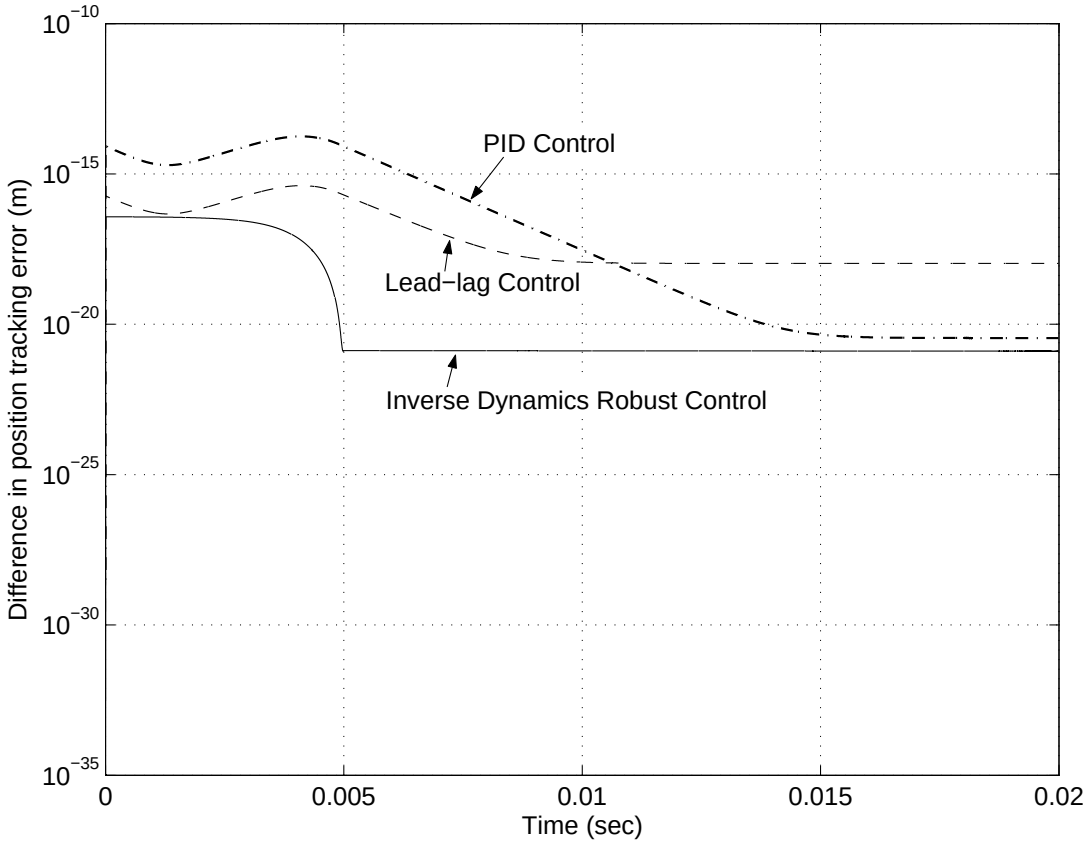

Figure 1.2: *Difference of position tracking error of different control methods*

1.4 Organization of the Thesis

This thesis consists of 8 chapters:

(i). **Chapter 1** gave a brief introduction to the background of the thesis and a overview of the work.

(ii). **Chapter 2** provides a literature review. It includes recent result on microscopic force sensing techniques, microgripper, piezoelectric actuator and micromanipulation system.

(iii). **Chapter 3** gives background about van der Waals force including the origin

of the force and some related issues. The van der Waals force formula between two spheres is also derived.

(iv). **Chapter 4** describes the micromanipulation system used in the simulations. The dynamic model of the system is derived. In addition, a desired trajectory and the parameters for the system model are determined. Simulation results are presented for the characteristics of the system and the effect of van der Waals force.

(v). **Chapter 5** describes the design of linear controllers, PID and lead-lag compensator. Simulations and results are presented.

(vi). **Chapter 6** focuses on inverse dynamics robust control of the system. The principle of the control algorithm is briefly introduced and the derivation of the control law for the micromanipulation is presented. The designed control law is applied for simulations. The results are discussed.

(vii). **Chapter 7** is the conclusion of the work.

Chapter 2

Literature Review on Micromanipulation

In this chapter, recent developments in the field of micromanipulation are reviewed. The first section describes several sensing techniques for force down to the resolution of a few nano Newtons. The techniques are important for micromanipulation systems especially when force feedback is required. The following section introduces some microgrippers with different actuating methods. A brief description of the properties and application of piezoelectric actuator is given next. The last section describes some recently developed manipulation systems and devices such as the model of pushing a sphere.

2.1 Microscopic Force Sensing Techniques

Measuring micro-force is important in the control of micromanipulation especially when force feedback is necessary. Since the force involved is less than a micro Newton, conventional force sensors are unsuitable. Precise sensing methods are required. Zhou et. al.[9] developed an optical beam deflection sensor which is based on a modified atomic force microscope. The sensor is integrated into a microgripper such that it can provide nanonewton level force feedback or

nanometric level position feedback. The force sensor is able to measure force as low as 2nN. The advantages of this sensing method are that it is insensitive to many of the sources of noise and it can be fabricated to meet the requirements for different force range and resolution. Another new force measurement technique is using Laser Raman Spectrophotometry [10]. It measures the stress of the micro structure instead of the displacement. The accuracy is expected to be better than μN order if the configuration of the device is designed properly. Micro strain gauge is also used for measurement [11], [12]. The resolution is not as good as the first two mentioned sensing methods. It is about 4μN in [11]. Zhang et. al. [13]-[15] used force transducer developed by Cambridge Technology Inc. to determine the properties of biological materials. The force transducer has a resolution of 0.01μN. Other methods used for force sensing in micromanipulation include piezoresistive, piezoelectric and piezomagnetic effects, as well as capacitive sensors [16].

2.2 Microgripper

The development of microgrippers has been an active research topic. Differences among the microgrippers include the material and actuators used and in fact most microgrippers designs closely depend on the materials used. With the help of the material properties and actuating mechanisms, better performance of the gripper can be achieved. In [17], shape memory alloy (SMA) is fabricated as one piece material which integrates the functionality of the device. Büttgenbach et. al.[18] used SMA as an micro-actuator in the microgripper as it has high power-to-volume ratio and ease of control. Kim et. al.[19] designed a polysilicon, electrostatic, comb-drive microgripper which has smooth, stable and controllable motion. Greitman et. al.[20] designed a microgripper using a thermal bimorph as actuator. The materials used for the bimorph are silicon and aluminium. Besides

thermal bimorph actuators, piezoelectric ceramic is also widely used to actuate microgrippers (more details of piezoceramics is given in the next section). As in [21], it is used in the flexure based designed microgripper to give precision positioning. Another microgripper designed with flexure hinges also employs the piezoelectric actuator for its high accuracy and reliability in producing displacements [22]. Some other gripping principles were introduced by Fischer et. al.[23], such as vacuum, adhesion, tong gripper with DC-motor and wire-loop gripper.

2.3 Piezoelectric Actuator

Piezoelectricity is a property of some materials that can transduce energy between electrical and mechanical domains. Applying an electric field across the piezoelectric materials produces mechanical strain and, conversely, application of mechanical stress on the materials induces electrical charge. This property can be found in ceramic materials, for example Lead Zirconate Titanate (PZT).

Piezoelectric ceramic is widely used as actuator in precision positioning systems requiring small displacements. Its characteristics of low mass, low heat generation, nonmagnetic and low cost as well as the ability of generating a large force with small displacements make it a favourite actuator for micromanipulation. The main drawback is the hysteretic behaviour.

Many forms of piezoceramics can be used. The most commonly are piezoplates and piezostacks. Wang et. al.[24] constructed a bimorph actuator from the piezoplates, which is able to provide linear displacement and a force of 0.8N. The

individual piezoplates can be made into a stack which provides larger displacement. This configuration increases the usage of piezoceramics. Newton et. al.[25] designed a linear piezoelectric motor using the piezostack actuators. It can perform a inchworm motion to move an object. The piezostacks can also be used in a translation stage which generates displacements with nanometer accuracy and a range of micro meters [26]. Nelson et. al.[27] used the piezostack actuator to operate a microgripper which is another example of using piezostack.

2.4 Micromanipulation Systems

In recent research in the field of micromanipulation, one of the most active areas is the influence of the adhesive forces on the system. The problems caused by the adhesive forces exist in micro object handling and motion control. Since in the microworld the gravitational force on the object is much smaller than the adhesive forces, the handling process, in particular the pick-up and release, is greatly affected. The micro object gripped by a microgripper often sticks to its finger and does not leave the finger when the gripper is opened [3]. Arai et. al.[6] proposed that the adhesive force can be reduced by increasing the surface roughness of the end-effectors. This can be done by adding 'micropyramids*' on the gripping surface of the fingers. Other methods to control the adhesive force are proposed in [2], such as controlling the moisture on end-effectors, controlling electrostatic forces, etc.

The adhesive forces also affect the dynamics of micromanipulation. Thus, modelling of adhesive forces is important and need to be considered for proper

*A sharp pyramid-like object which can generate high electric field that reduces electrostatic forces. It is also effective for reducing the van der Waals force.

control and planning of micromanipulation. Rollot et. al.[8] modelled and simulated the pick-up and release of a micro-sphere in the influence of other spheres. They presented different handling results in terms of different combination of materials, size of spheres and speed of end-effector. Zhou et. al.[28] studied the task of pushing a micro-sphere. Pushing work was also studied in [4] and [29]. In contrast to [28] which only simulated the dynamic of the pushing, they developed force control algorithms and implemented the operation.

Besides pushing, several systems were developed to assemble micro-devices, manipulate biological cells, etc. Zhou et. al.[7] developed a microgripper to study the force controlled gripping of micro-objects. Tanikawa et. al.[30] designed a two-fingered micro-hand for manipulating micro-parts such as white blood cells of humans. Nakamura et. al.[31] showed a one-finger system which is able to draw a circle less than 1mm diameter.

A lot of research have been carrying out in the micromanipulation area. This indicates that the existing control methods and devices including grippers and sensors used for macroscopic systems are not suitable to be applied on the microscopic systems. The major consideration in the literature is microscopic forces. It is the main factor that causes the difference of macro and micro systems. Thus finding the method to attenuate the microscopic forces is an important work to achieve good system performance. The papers showed that much research have been done on hardware for this purpose. Novel grippers and manipulation planning were developed. On the contrary, this thesis focuses on the 'software' aspect in dealing with the microscopic forces.

Chapter 3

Van der Waals Force

3.1 Introduction

This thesis deals with the effect of microscopic forces in micromanipulation systems. It is necessary to study the microscopic forces in detail. Microscopic forces usually refer to forces of which magnitudes are smaller than one micro-Newton (μN). In the field of micro-robotics, the adhesive forces, which are microscopic forces have been actively investigated due to their influence on the system motion. The adhesive forces include van der Waals force, electrostatic force, surface tension and others. As mentioned in Chapter 1, this project focuses on the van der Waals force. The influence of this force occurs not only while two objects touch each other (distance between surface of molecules about 0.16nm), but also when they are at a certain distance up to 5nm. It affects the micromanipulation system dynamics significantly.

The van der Waals force has been studied for more than 200 years. The study of the van der Waals force started from the observation of the wetting of solids by liquids in the early 1700s. In the 1800s, many scientists were interested in the behaviour of liquids, in particular, the phenomena of wetting and capillarity. In the 1930s, London [32], using advances of the quantum mechanics, demonstrated

that the van der Waals force is a result of transient-induced dipoles. He showed that the induced dipoles result from the intrinsic polarizability of the interatomic bonds and the presence of a propagating electromagnetic field are long range and do not disappear at high temperatures. In the same decade, Hamaker [33] extended the study of London by summing the point-by-point interactions among molecules and producing a measure of the net attraction of two separate bodies. This led to the development of the Hamaker constant in establishing the magnitude of the van der Waals force.

The concept developed by London is described in Section 3.2, which also includes the origin of van der Waals force. It is followed by a description of the retardation effect. Hamaker's work is introduced in the fourth section. The last section is the derivation of the van der Waals force formulas between two spheres.

3.2 Origin of van der Waals Force

The long-range van der Waals force between atoms or molecules in materials result from the interaction of dipoles. For uncharged molecules consisting of a permanent or induced dipole, the van der Waals forces can be considered as a result of three additive terms – the Keesom force, the Debye force, and the London force, as shown in Eq. (3.1).

$$F_{vdW} = F_{Keesom} + F_{Debye} + F_{London} \tag{3.1}$$

(i). Keesom Force (Orientation Effect): For two permanent dipoles, the interaction of the dipole's electric fields results in either an attractive force when the dipoles are antiparallel, or a repulsive force when the dipoles are parallel. This force vanishes when temperature increases since thermally induced motions of permanent dipoles can disorder the mutual alignment at high temperature.

(ii). Debye Force (Induction Effect): For a molecule consisting of a permanent dipole, it can induce a dipole moment in the electron cloud of another atom or molecule. These induced electronic dipole moments can interact with the permanent dipolar molecule. This interaction energy results in the Debye force. It requires at least one permanent dipole.

(iii). London Force (Dispersion Effect): Since the Keesom and Debye forces require the presence of permanent dipole moments, London pointed out that they cannot be solely the forces contributing to the van der Waals forces. London utilized an idea from quantum mechanics, which stated that an electron, even in its ground state and at absolute zero temperature, universally exhibits a zero point motion. This zero point motion of the electron results in a propagating electromagnetic wave such that their associated fields can induce dipole moments in the electron clouds of nearby atoms or molecules. It is these induced-dipole and induced-dipole interactions that forms the attractive force which is the basis of the London force.

Comparison of the contributions of these three forces shows that the London force dominates [34], i.e. the dispersion effect has the largest proportion in the van der Waals forces. This force is independent of temperature and does not require a permanent dipole.

London's equation describes the dispersion interaction energy between two identical atoms or molecules, i.e.,

$$W(r) = -\frac{\lambda}{r^6} = -\frac{3\alpha_0^2 hv}{4(4\pi\varepsilon_0)^2 r^6} \tag{3.2}$$

where

r = distance between two atoms or molecules,
$\lambda = \dfrac{3\alpha_0^2 hv}{4(4\pi\varepsilon_0)^2}$, London-van der Waals constant,

α_0 = electronic polarizability,

h = Planck's constant,

v = orbiting frequency of the electron,

ε_0 = permittivity of free space.

This equation was derived by London in 1937 using quantum mechanics. It will be used to compute the van der Waals force between two objects in later sections. More details of the origin of the van der Waals force can be found in Israelachvili[34] and French[35] or any quantum mechanics textbook.

3.3 Retardation Effect

For two molecules in free space, retardation effect begins at a separation greater than 5nm. In the van der Waals force formula derived theoretically such as the one in the later Section 3.5, this effect is normally not considered. Hence, the van der Waals force is always overestimated for separations above 5nm. The retardation is not linear and the derivation of the actual retarded van der Waals force is very complex.

The retardation effect is due to the longer transit time of the electromagnetic wave between the dipoles. When the distance is small, this transit time can be neglected. However, when the distance between two dipoles increases, the transit time of the two electromagnetic waves become longer causing the highest energy interatomic bands out of phase, which reduces their contributions to the dispersion interaction.

In this project, the system studied is set such that the separation between two objects is below 5nm, so that the retardation effect of the van der Waals force is neglected. Therefore, only non-retarded van der Waals forces are considered.

3.4 Hamaker Constant

In determining the van der Waals interaction energy and force between two bodies, it is always assumed that the interaction is *non-retarded* and *additive*. With the assumption of the additivity property, Hamaker [33] was able to determine the van der Waals force between two spherical particles by summing all dipolar interactions of the atoms or molecules of the particles. He introduced a constant A in his work which was later named as the Hamaker constant and is widely used in the study of van der Waals force. The Hamaker constant is a function of the material properties and is defined as

$$A = \pi^2 q_1 q_2 \lambda_{12} \tag{3.3}$$

where q_1, q_2 are the number of atoms per unit volume in the two interacting bodies, λ_{12} is the London-van der Waals constant for the pairs of atoms indicated by the subscript. It is positive for an attractive force and negative for a repulsive force. The unit of the Hamaker constant is Joule and its value is generally in the range of $0.4 \sim 4{\times}10^{-19}$J. In [33], Hamaker proved that the van der Waals forces between two particles of the same material are always attractive. He also stated that if the particles are of different composition, the resultant force may be attractive or repulsive.

One important property of the Hamaker constant is the combining relations (or combining laws). It is useful in obtaining approximate values for unknown Hamaker constants in terms of known ones. It states that if A_{132} is defined as the non-retarded Hamaker constant for media 1 and 2 interacting across medium 3, A_{132} may be approximately related to A_{131} and A_{232} as

$$A_{132} \approx \pm\sqrt{A_{131} A_{232}} \tag{3.4}$$

From this, we have

$$A_{12} \approx \sqrt{A_{11} A_{22}} \tag{3.5}$$

where A_{12} is for media 1 and 2 interacting across vacuum, i.e., with no medium 3 in between.

3.5 The van der Waals force between two spheres of same material

The derivation of the van der Waals forces between objects starts from London's equation (3.2), the dispersion interaction energy between two atoms or molecules. By assuming the additivity of the interaction energy, the total dispersion interaction energy between two objects can be obtained. Hamaker [33] derived the formula of dispersion energy of interaction between two spheres, shown in Figure 3.1, as

$$W = -\frac{A}{6}\left[\frac{2R_1R_2}{C^2-(R_1+R_2)^2} + \frac{2R_1R_2}{C^2-(R_1-R_2)^2} + \ln\frac{C^2-(R_1+R_2)^2}{C^2-(R_1-R_2)^2}\right] \tag{3.6}$$

where

$A = \pi^2 q^2 \lambda$, Hamaker constant of the material,

q = number of atoms or molecules per unit volume,

λ = London-van der Waals constant,

R_1, R_2 = radii of the two spheres,

C = distance between the spheres' centres.

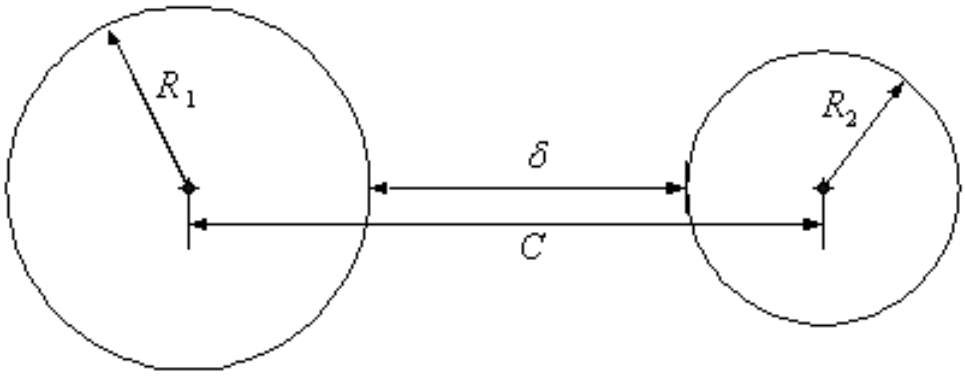

Figure 3.1: *Notation for two spheres in interaction*

The van der Waals force of the two spheres can be obtained by differentiating this formula with respect to the distance C.

$$\begin{aligned}
\frac{\partial W}{\partial C} &= -\frac{A}{6}\left\{\frac{-2R_1R_2\times 2C}{[C^2-(R_1+R_2)^2]^2}+\frac{-2R_1R_2\times 2C}{[C^2-(R_1-R_2)^2]^2}+\right.\\
&\qquad\left.+\frac{2C}{C^2-(R_1+R_2)^2}-\frac{2C}{C^2-(R_1-R_2)^2}\right\}\\
&= -\frac{AC}{3}\left\{\frac{-2R_1R_2}{[C^2-(R_1+R_2)^2]^2}+\frac{-2R_1R_2}{[C^2-(R_1-R_2)^2]^2}+\right.\\
&\qquad\left.+\frac{C^2-(R_1-2R_1R_2+R_2^2)-C^2+(R_1^2+2R_1R_2+R_2^2)}{[C^2-(R_1+R_2)^2][C^2-(R_1-R_2)^2]}\right\}\\
&= \frac{AC\times 2R_1R_2}{3}\left\{\frac{1}{[C^2-(R_1+R_2)^2]^2}+\frac{1}{[C^2-(R_1-R_2)^2]^2}-\right.\\
&\qquad\left.-\frac{2}{[C^2-(R_1+R_2)^2][C^2-(R_1-R_2)^2]}\right\}\\
&= \frac{2ACR_1R_2}{3}\left\{\frac{1}{[C^2-(R_1+R_2)^2]^2[C^2-(R_1-R_2)^2]^2}\right\}\left\{[C^2-(R_1-R_2)^2]^2+\right.\\
&\qquad\left.+[C^2-(R_1+R_2)^2]^2-2[C^2-(R_1+R_2)^2][C^2-(R_1-R_2)^2]\right\}\\
&= \frac{2ACR_1R_2}{3}\left\{\frac{[C^2-(R_1-R_2)^2-C^2+(R_1+R_2)^2]^2}{[C^2-(R_1+R_2)^2]^2\,[C^2-(R_1-R_2)^2]^2}\right\}\\
F &= \frac{ACR_1R_2}{3}\left\{\frac{32R_1^2R_2^2}{[C^2-(R_1+R_2)^2]^2\,[C^2-(R_1-R_2)^2]^2}\right\} \qquad (3.7)
\end{aligned}$$

This is the non-retarded van der Waals force between two macroscopic spheres. Expression in term of the nearest surface separation δ can also be obtained by

substituting $C = R_1 + R_2 + \delta$ into Eq. (3.7). The force becomes

$$\begin{aligned} F &= \frac{32A(R_1 + R_2 + \delta)R_1^3 R_2^3}{3[(C + R_1 + R_2)(C - R_1 - R_2)]^2\,[(C + R_1 - R_2)(C - R_1 + R_2)]^2} \\ &= \frac{32A(R_1 + R_2 + \delta)R_1^3 R_2^3}{3(2R_1 + 2R_2 + \delta)^2\,\delta^2\,(2R_1 + \delta)^2\,(2R_2 + \delta)^2} \end{aligned} \tag{3.8}$$

Chapter 4

Development of a Micromanipulation System

The general system described in Section 1.2 is not sufficient to explore the control of micromanipulation system. A more concrete system has to be developed which is developed in this chapter. This chapter presents the configuration and modelling of the micromanipulation system, including the materials, geometry and devices assumed. The interaction of the system with the van der Waals force is also considered. System parameters to run the simulation are determined according to the system configuration and a desired trajectory is selected. Several simulations are conducted on the system to observe its characteristics and the effect of the van der Waals force on the system.

4.1 System Configuration

Consider a micro-assembly task as shown in Figure 4.1. Two spheres B and C are fixed on a substrate. Sphere A is held stationary by a tool at an initial height. From that starting height, sphere A is moved down to 'touch' spheres B and C. The range of movement is set to be few nanometers. During the maneuver, motion trajectory and velocity of sphere A are affected by the van der Waals force between

the spheres B, C and A. This motion is to be controlled.

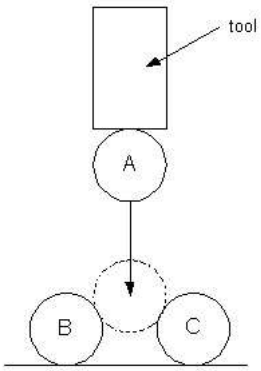

Figure 4.1: *System Configuration*

The tool is assumed to include a piezoelectric stack actuator and a microgripper which holds the sphere firmly throughout the whole process. The reasons of using the piezostack are its advantage in giving precise displacement and force and, also, the ease of control. It is assumed that its hysteretic behaviour is negligible and the dynamics of the piezostack is linear.

The spheres in the system are set to be identical, i.e. of same material and same radius. When the spheres are in contact, it means the separation of spheres is 0.165nm from surface to surface. This is called the contact distance. (refer to [34])

4.2 Model of Piezoelectric Stack Actuator

The modelling of the piezoelectric stack can be found in [26] and [36]. It can be modelled as a simple mass-damper-spring system as shown in Figure 4.2, where m_p, c and k_p are the mass, damping coefficient and stiffness of the piezostack

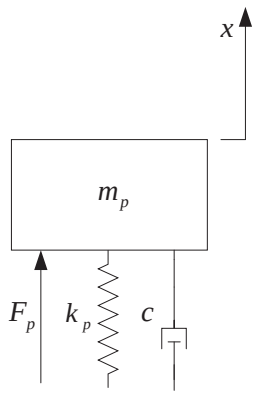

Figure 4.2: *Model of piezoelectric stack*

respectively, and F_p is the force transduced from the electrical input. The piezoelectric element converts the input voltage to force. If the input voltage is V, the transduced force F_p can be calculated as

$$F_p = N k_p \, d_{33} V \tag{4.1}$$

where

d_{33} = piezoeletric charge constant,

N = number of piezodiscs which make up the stack.

4.3 Dynamic Model of the System

According to the system configuration and the piezostack model, a free body diagram of the system is obtained, as shown in Figure 4.3, where M is the mass including the masses of piezostack, sphere A and the tool holding it, c, k_p and F_p are as mentioned above, F_v is the vertical component of van der Waals force between spheres and x is the position of mass from equilibrium position.

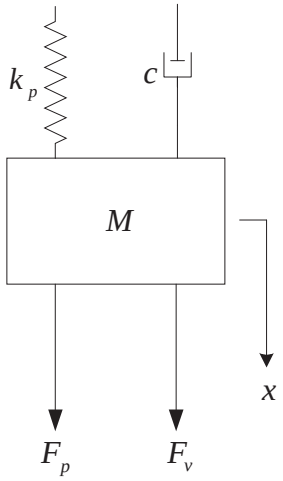

Figure 4.3: *Free body diagram of the system*

The dynamic equation of the system is

$$M\ddot{x} + c\dot{x} + k_p x = F_p + F_v \tag{4.2}$$

The derivation of F_v is as follow. Referring to Figure 4.4, recall that the van der Waals force between two spheres is expressed as Equation (3.7)

$$F_{vdw} = \frac{32ACR_1^3R_2^3}{3\left[C^2 - (R_1 + R_2)^2\right]^2\left[C^2 - (R_1 - R_2)^2\right]^2}$$

Since two spheres B and C are identical, the van der Waals forces exerted on A by B and C have the same magnitude. The horizontal components F_h are cancelled due to the symmetry of the configuration. The remaining force is the vertical component of the van der Waals force F_{vdw}.

$$
\begin{aligned}
F_v &= 2 \times \frac{32ACR_1^3R_2^3}{3\left[C^2-(R_1+R_2)^2\right]^2\left[C^2-(R_1-R_2)^2\right]^2} \times \cos\theta \\
&= \frac{64AR^6C}{3\left[C^2-4R^2\right]^2\left[C^2\right]^2} \times \cos\theta \\
&= \frac{64AR^6C}{3\left[C^2-4R^2\right]^2\left[C^2\right]^2} \times \frac{D-x}{C} \\
&= \frac{64AR^6(D-x)}{3\left[(D-x)^2+l^2-4R^2\right]^2\left[(D-x)^2+l^2\right]^2}
\end{aligned} \tag{4.3}
$$

as $R_1 = R_2 = R$ and $C^2 = (D-x)^2 + l^2$. Substituting (4.3) into Equation (4.2) gives

$$
M\ddot{x} + c\dot{x} + k_p x = k_p\, d_{33}\, NV + \frac{64AR^6(D-x)}{3\left[(D-x)^2+l^2-4R^2\right]^2\left[(D-x)^2+l^2\right]^2} \tag{4.4}
$$

Equation (4.4) is the dynamics model of the micromanipulation system with the van der Waals force.

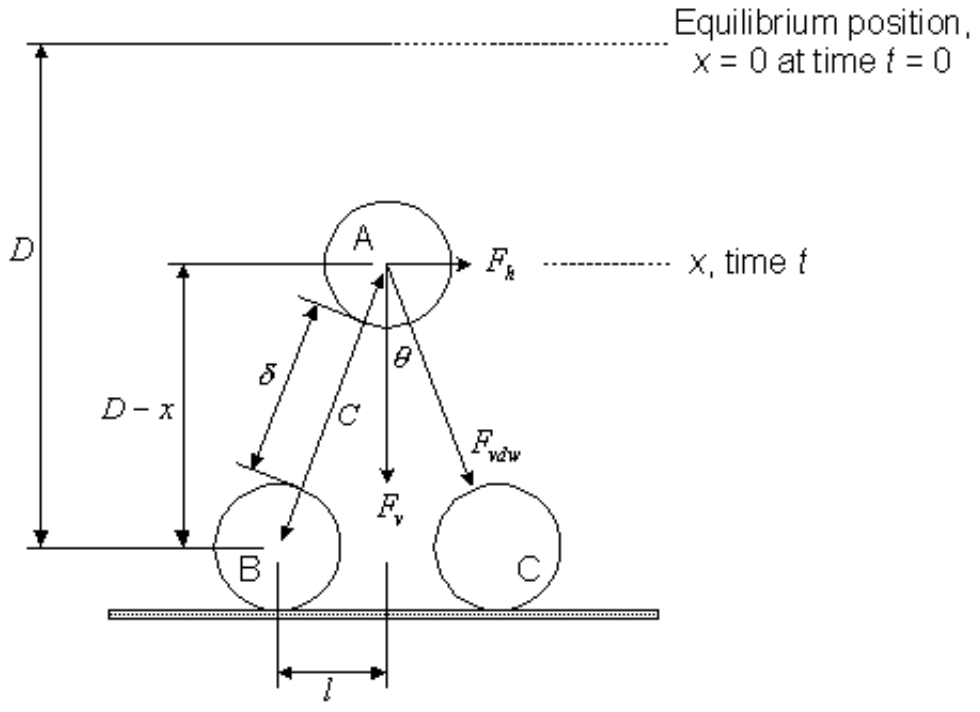

Figure 4.4: *Van der Waals force between two spheres*

4.4 Parameters Calculation

4.4.1 Spheres Parameters

Assuming that the spheres are made of Silicon Dioxide (SiO_2). The properties of SiO_2 and other parameters are

Sphere Parameter	Symbol	Numerical Value
Radius	R	10 μm
Non-retarded Hamaker Constant	A_{SiO_2}	6.5×10^{-20} J
Density (dry)	ρ_{SiO_2}	2270 kg/m^3
Young's Modulus	E_{SiO_2}	73 GPa
Mass of the sphere	m_s	9.5086×10^{-12} kg

Table 4.1: *Sphere parameters for simulations*

4.4.2 Piezostack Parameters

There are many types of ceramic that can be used as piezoelectric material. A common type – PZT (Lead Zirconate Titanate) is employed here. Its properties are listed below.

PZT Property	Symbol	Numerical Value
Piezoelectric charge constant	d_{33}	500×10^{-12} m/V
Young's Modulus	E_{PZT}	6×10^{10} Pa
Density	ρ_{PZT}	7.5×10^3 kg/m^3
Maximum electrical field strength	B_{max}	2kV/mm

Table 4.2: *Material properties of PZT for simulations*

The usual operating condition of the piezostack is under an electrical field strength of 1kV/mm to 2kV/mm and at maximum voltage of 150V (low voltage actuator) or 1000V (high voltage actuator). In this project, it is set that the piezostack works under electrical field strength of 1kV/mm and at voltage between ±150V. Parameters of the piezostack can be determined as below:
Let the maximum operating voltage be $V_{max} = 150$ V. The maximum extension of a piezodisc at 150V can be calculated as

$$\begin{aligned} \text{Max. extension} &= d_{33} \times 150 \\ &= 500 \times 10^{-12} \times 150 \\ &= 7.5 \times 10^{-8} \ \text{(m)} \end{aligned}$$

The thickness of the piezodisc for it to be operated at $B = 1$kV/mm electric field strength is

$$\text{thickness} = \frac{V_{max}}{B} = 0.15 \ \text{(mm)}$$

It is set that there are 10 piezodiscs to make up the piezostack, so the length of the piezostack is

$$L = 0.15 \times 10 = 1.5 \ \text{(mm)}$$

Hence, the maximum extension is 7.5×10^{-7}m, i.e. max. strain = 0.05%. If the radius of the piezostack is set as $r_p = 8\mu\text{m} = 8 \times 10^{-6}$ m. The stiffness of the piezostack can be calculated as

$$k_p = \frac{\pi \, r_p^2 \, E_{SiO_2}}{L} \approx 8 \times 10^3 \ \text{(N/m)}$$

Mass of the piezostack is

$$m_p = \pi \, r_p^2 \, L \rho_{SiO_2} = 2.2619 \times 10^{-9} \ \text{(kg)}$$

4.4.3 Microgripper Parameters

As mentioned in Section 2.1, Zhou et. al. [7] introduced a new force sensing method using optical beam deflection (OBD) and described a microgripper with built-in OBD force sensor. In this project, it is assumed that a similar microgripper is used. Figure 4.5 illustrates the simple model of the microgripper. The cantilever finger ('a') is used to measure the gripping force by using laser beam. Microfinger ('b') should have a higher stiffness so that almost all deflection is taken up by the cantilever finger to give a higher accuracy measurement.

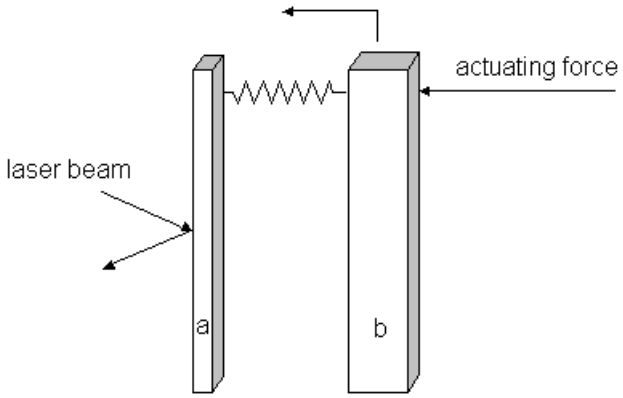

Figure 4.5: *Model of microgripper*

Let the commonly used Silicon Nitride (Si_3N_4) be the material of the fingers. The properties are

$E_{Si_3N_4}$ Property	Symbol	Numerical Value
Young's Modulus	$E_{Si_3N_4}$	304GPa
Density	$\rho_{Si_3N_4}$	3400 kg/m^3
Non-retarded Hamaker constant	$A_{Si_3N_4}$	1.92×10^{-19} J

Table 4.3: *Material properties of Si_3N_4 for simulations*

Table 4.4 shows the dimension and calculated mass of the two fingers. The values are set corresponding to the size of the sphere.

Finger	Dimensions	Mass
Cantilever	500μm $\times$ 2μm $\times$ 30μm	1.02×10^{-10} kg
Microfinger	500μm $\times$ 10μm $\times$ 30μm	5.1×10^{-10} kg

Table 4.4: *Parameter of microgripper fingers*

4.4.4 System Parameters and Transfer Function

The mass of the whole system, M, includes the mass of piezostack actuator, microgripper and sphere. It is approximated as

$$\begin{aligned} M &= \text{sphere mass} + \text{piezostack mass} + \text{microgripper fingers mass} \\ &= 9.5086\times10^{-12} + 2.2619\times10^{-9} + 1.02\times10^{-10} + 5.1\times10^{-10} \\ &= 2.8834\times10^{-9} \\ &\approx 3\times10^{-9}\ \text{(kg)} \end{aligned}$$

The system parameters in Equation (4.4) for simulations are summarized in the Table 4.5 below, see also Figure 4.4.

Note that the distance D is set within the extension range of the piezostack actuator depending on the desired system motion. Once the system displacement is designed, D can be determined. l is the configuration setting.

The transfer function of the system without the van der Waals forces between spheres, F_v, can be derived from Equation (4.4):

$$\begin{aligned} M\ddot{x} + c\dot{x} + k_p x &= F_p \\ Ms^2X(s) + csX(s) + k_pX(s) &= k_p\, d_{33} NV(s) \\ \frac{X(s)}{V(s)} &= \frac{k_p\, d_{33} N}{Ms^2 + cs + k_p} \end{aligned} \tag{4.5}$$

Parameter	Value
k_p	8000 N/m
d_{33}	500×10^{-12} m/V
N	10
M	3×10^{-9} kg
c	5 Ns/m
$A(A_{SiO_2})$	6.5×10^{-20} J
l	1.999×10^{-5} m
R	10 μm

Table 4.5: *Parameters of the system dynamics model*

4.5 System Characteristics

Substituting the parameters into Equation (4.5) gives the system transfer function without van der Waals force

$$\frac{X(s)}{V(s)} = \frac{4\times10^{-5}}{3\times10^{-9}s^2 + 5s + 8000} \tag{4.6}$$

In order to examine the system characteristics and check the validity of the system dynamic model, simulations are run on the modelled system using MathWorks Simulink® in the MATLAB program. Simulink is a graphical interface to Matlab using block diagram and connectors.

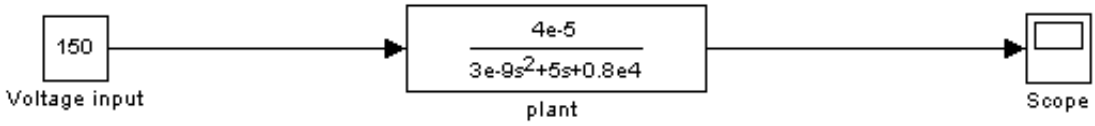

Figure 4.6: *Simulation model for the open loop system with 150V input*

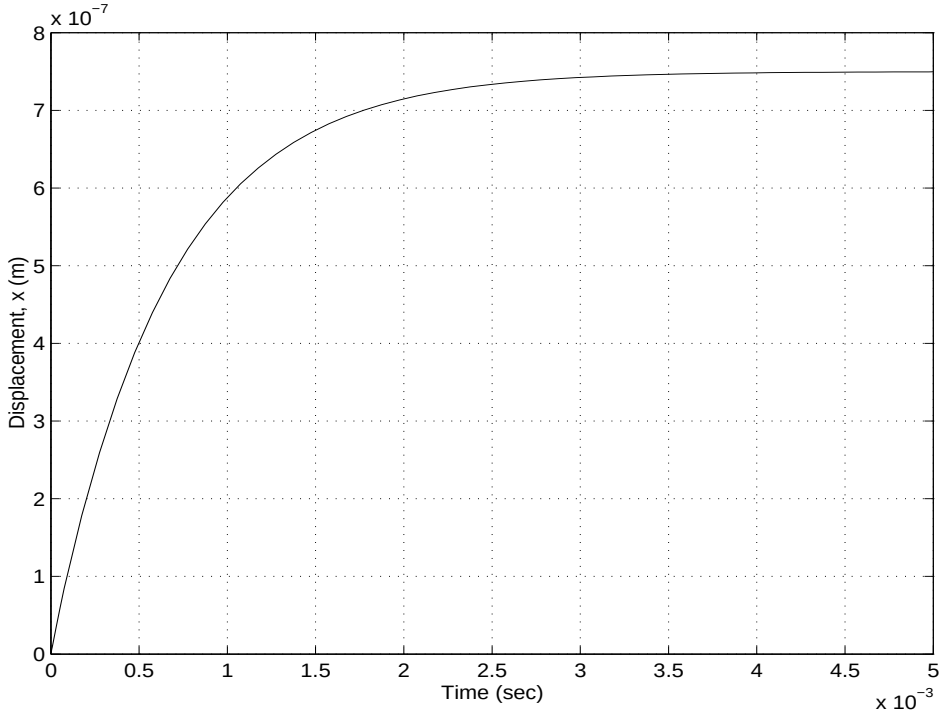

Figure 4.7: *System response with 150V input*

The first simulation is to input a voltage of 150V to the open loop system. Figure 4.6 shows the Simulink model for the simulation. The time for simulation is set to be 0.005sec. The simulation result is shown in Figure 4.7 which plots the displacement of the system x (also the extension of the piezostack). The steady state value is 7.5×10^{-7}m which is the same as the calculated maximum extension value (see Section 4.4.2). The next simulation is a step response of the open loop system. The result is shown in Figure 4.8. The settling time is 0.00245 sec and no overshoot is observed. The steady state value is 5×10^{-9}m which is the extension of piezostack at 1V input voltage. Recall that the piezoelectric charge constant d_{33}, defined as the extension of piezoelectric material per volt, is 5×10^{-10}m. Since the piezostack is made of 10 piezodisc, 1V applied to the piezostack will provide an extension of 5×10^{-9}m ($= 5\times10^{-10}\times 10$). It matches the steady state value of the model step response.

Both simulation results show that the extensions of the piezostack of the model agree with the calculated values. Hence, the system dynamics model developed is valid. This dynamic model is used as the micromanipulation system for examining the influence of van der Waals force. The fast response and zero overshoot indicate that the system is capable to perform well.

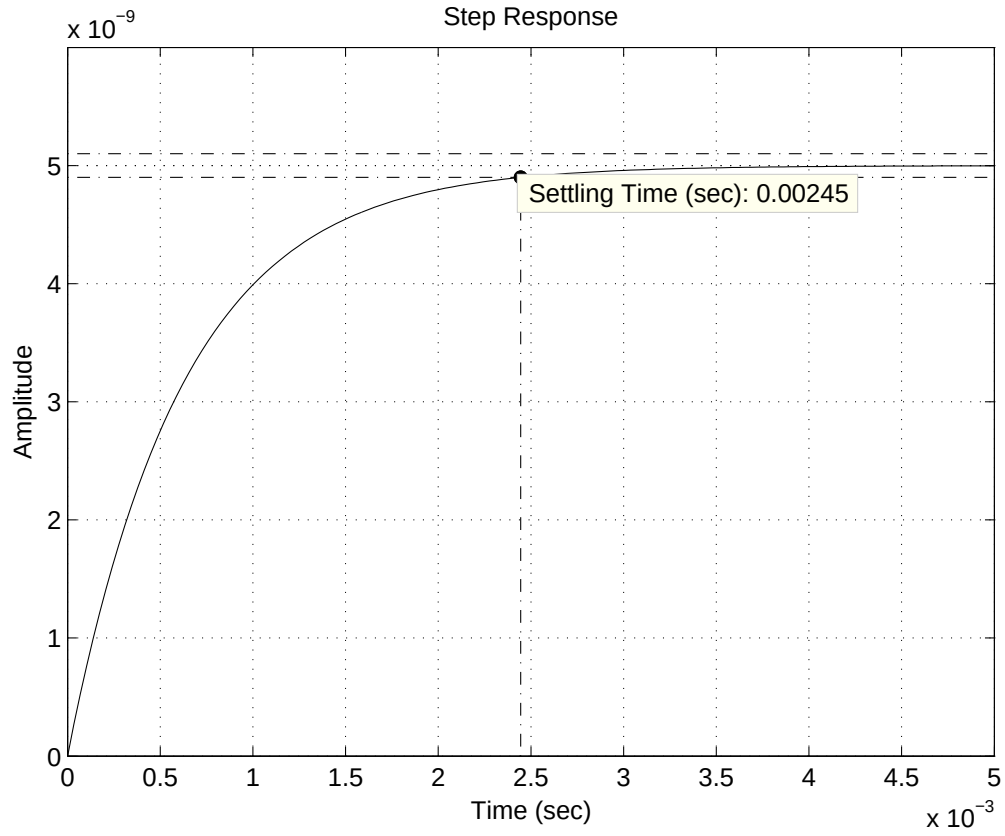

Figure 4.8: *Step response of system*

4.6 Trajectory for Simulation

For all the simulations in this project, a trajectory is used as reference input instead of solely using step input. This is better in showing the effect of van der

Waals force. The trajectory is the motion of the sphere A. Referring to Figure 4.4, at the beginning, sphere A is held at initial height D. The initial velocity is zero. The sphere A is set to be moved downwards for 10nm to touch the sphere B and C which means that the final distance between the surfaces of spheres A and B, C is 0.165nm. At that distance, the two spheres are considered in contact [34]. The sphere is then held at the final position for the rest of the simulation time. The time to move the sphere from the initial position to the final position is 0.005sec.

Let $x_f = 10$nm be the final position and C_f be the final distance between two spheres centers. Referring to Fig. 4.4, D is obtained as

$$\begin{aligned} C_f &= 2R + 0.165\times10^{-9} \\ &= 2 \times 10\times10^{-6} + 0.165\times10^{-9} \\ &= 2.0000165\times10^{-5} \\ D - x_f &= \sqrt{C_f^2 - l^2} \\ D &= \sqrt{C_f^2 - l^2} + x_f \\ &= \sqrt{(2.0000165\times10^{-5})^2 - (1.999\times10^{-5})^2} + 10\times10^{-9} \\ &= 6.4757355\times10^{-7} \end{aligned}$$

We use as desired trajectory a fifth order polynomial with boundary conditions:

At starting time $t_0 = 0$ sec, $x_0 = 0$ m, $\dot{x}_0 = 0$ m/s, $\ddot{x}_0 = 0$ m/s^2;

At finishing time $t_f = 0.005$ sec, $x_f = 10\times10^{-9}$ m, $\dot{x}_f = 0$ m/s, $\ddot{x}_f = 0$ m/s^2.

The resulting trajectory is

$$x(t) = 0.8t^3 - 240t^4 + 19200t^5 \tag{4.7}$$

Figure 4.9 shows the trajectory of x from 0 sec to 0.005 sec. After 0.005 sec, the position x is held at the final position $x_f = 10\times10^{-9}$m.

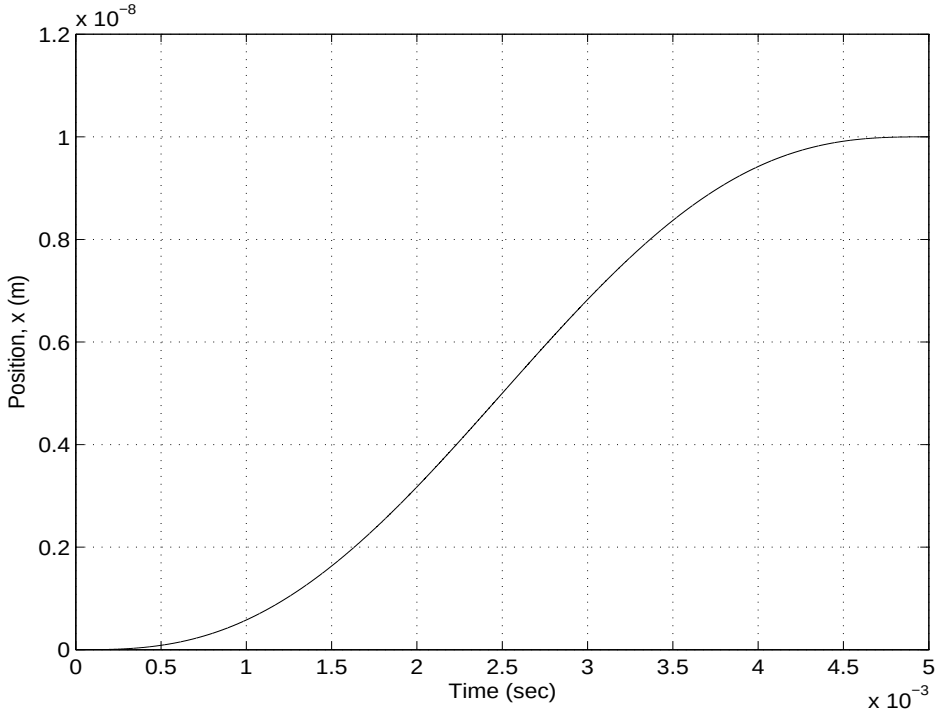

Figure 4.9: *Desired trajectory used for feedback loop simulation*

4.7 Effect of van der Waals Force

4.7.1 Closed-loop Step Response

To examine the effect of van der Waals force on the system, simulations are run of the closed-loop feedback system with the trajectory input. The feedback system requires a gain for position tracking. The system response should have an overshoot smaller than 1% and low position error. The low overshoot is needed to prevent collision of the spheres since the motion of sphere is designed to move and touch the other sphere. Step reference input is used to determined the gain. Then the gain is used for the system simulations with trajectory input.

The steady state error of the closed-loop step response of the system can be derived analytically. Referring to Figure 4.10, ignoring the van der Waals force

influence, position error E can be derived as

$$\begin{aligned} E &= R - Y \\ &= R - TR \\ &= (1 - T)R \\ &= \left(1 - \frac{KG}{1 + KG}\right) R \\ &= \left(\frac{1}{1 + KG}\right) R \end{aligned} \tag{4.8}$$

where

R = reference input,

Y = output,

T = closed-loop system transfer function,

K = feedback gain,

G = plant transfer function Eq. (4.5).

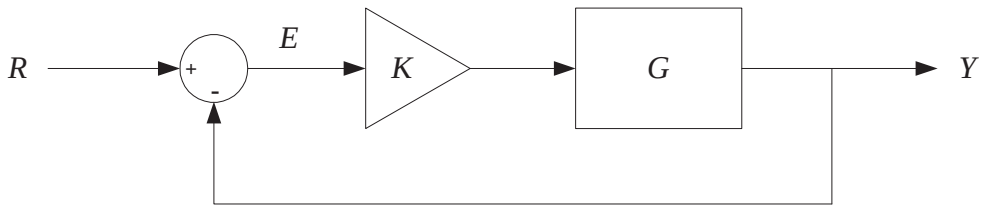

Figure 4.10: *Illustration of closed-loop system*

For a step reference input, R = 1/s, steady state error is obtained by using Final Value Theorem.

$$
\begin{aligned}
E_{ss} &= \lim_{s\to 0} s\left(\frac{1}{1+KG}\right)\left(\frac{1}{s}\right) \\
&= \lim_{s\to 0} \frac{1}{1+K\left(\dfrac{k_p\, d_{33} N}{Ms^2+cs+k_p}\right)} \\
&= \lim_{s\to 0} \frac{Ms^2+cs+k_p}{Ms^2+cs+k_p+k_p\, d_{33} NK} \\
&= \frac{k_p}{k_p+k_p\, d_{33} NK} \\
&= \frac{1}{1+d_{33} NK} \qquad (4.9)
\end{aligned}
$$

Equation (4.9) shows that larger gain used gives smaller steady state error. However, the error is never eliminated. To have zero error, a more sophisticated controller must be employed.

A gain is chosen to give a small error and zero overshoot for the simulations in this section. The gain obtained is 1×10^{13}. Figure 4.11 shows the system response obtained from simulation. The settling time is 4.71×10^{-8} sec and overshoot is zero. The steady state error is 2×10^{-5} m. With this result, the feedback gain should be able to provide low error and zero overshoot response for the system with trajectory input.

4.7.2 System Response to Trajectory Input

To observe how the system evolves when the van der Waals force is not modelled, the feedback system is simulated with trajectory as reference input and without van der Waals force interruption. It is to see that if the van der Waals force is not modelled in the system, how it actually acts in the system. Figure 4.12 shows the simulink model of the system. The simulation time range of 0.01 sec and the solver ode15s are used. The system response, position x, is shown in Figure 4.13. There is no overshoot in the response. The position x is used to calculate the van

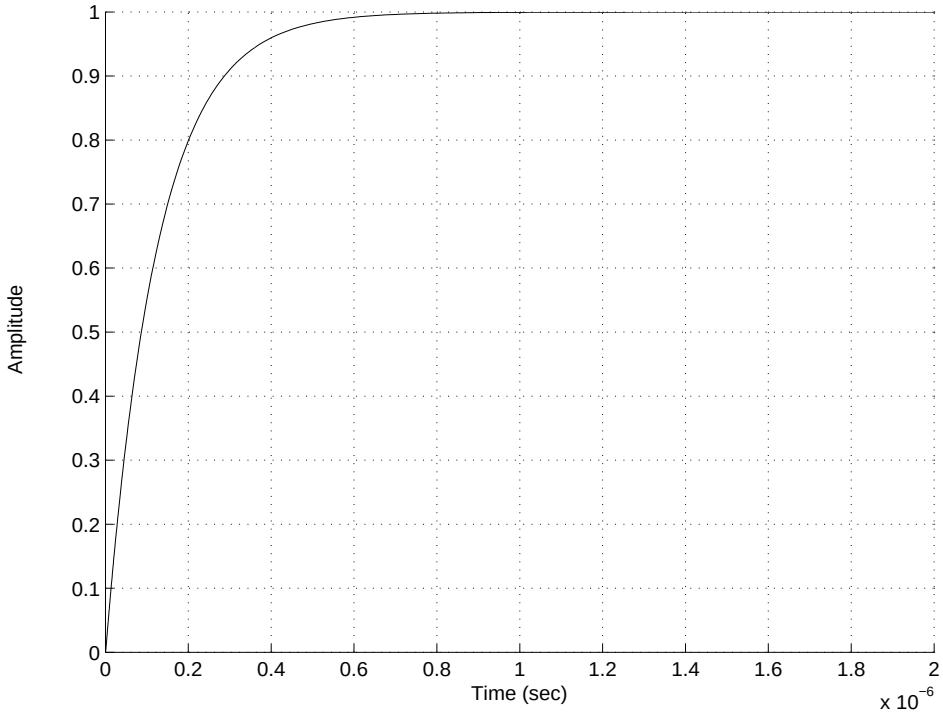

Figure 4.11: *Closed-loop step response of system*

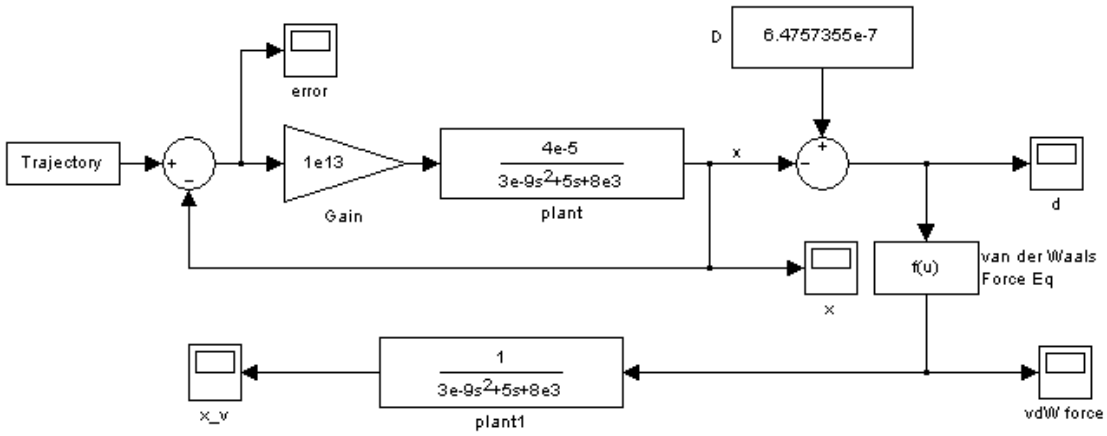

Figure 4.12: *Simulation model of feedback system with trajectory input*

der Waals force with the Equation (4.3). Then the displacement of the sphere A caused by the van der Waals force can be obtained by inputting the van der Waals

force into the plant transfer function (Eq. (4.6)). Figure 4.14 shows the position tracking error. Notice that the steady state error is a constant. It is expected since only feedback gain is used (refer to the steady state error derived above).

Figure 4.15 shows the van der Waals force, F_v, and the distance, δ, between surfaces of spheres A and B or C. In the process, the δ starts from about 0.4863nm and reduces to 0.165nm, which is the contact distance. The van der Waals force increases as the two spheres come closer to each other. When the spheres are in contact, the van der Waals force reaches its maximum value. During the motion, the van der Waals force attracts the sphere A and tries to pull it downwards. Figure 4.16 shows the displacement of sphere A due to the van der Waals force. Let this displacement be x_v. From the collected data, the ratio of x_v to x can be calculated. At steady state, the percentage of the ratio of x_v to x is 0.1585%. This error caused by the van der Waals force can affect the system performance since high accuracy is required in micromanipulation. We conclude that more sophisticated control law is to be applied to reduce van der Waals force effect and obtain lower position tracking error. Further van der Waals force model may be considered as the part of control law design so that the control law is more effective in reducing the van der Waals force effect.

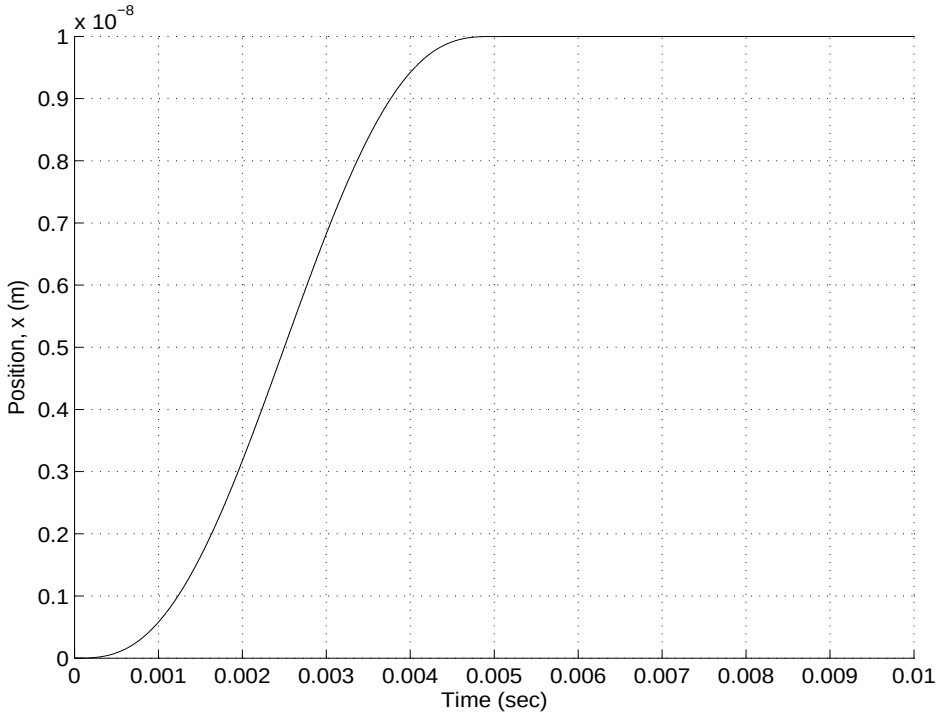

Figure 4.13: *Position x for the negative feedback system without van der Waals force*

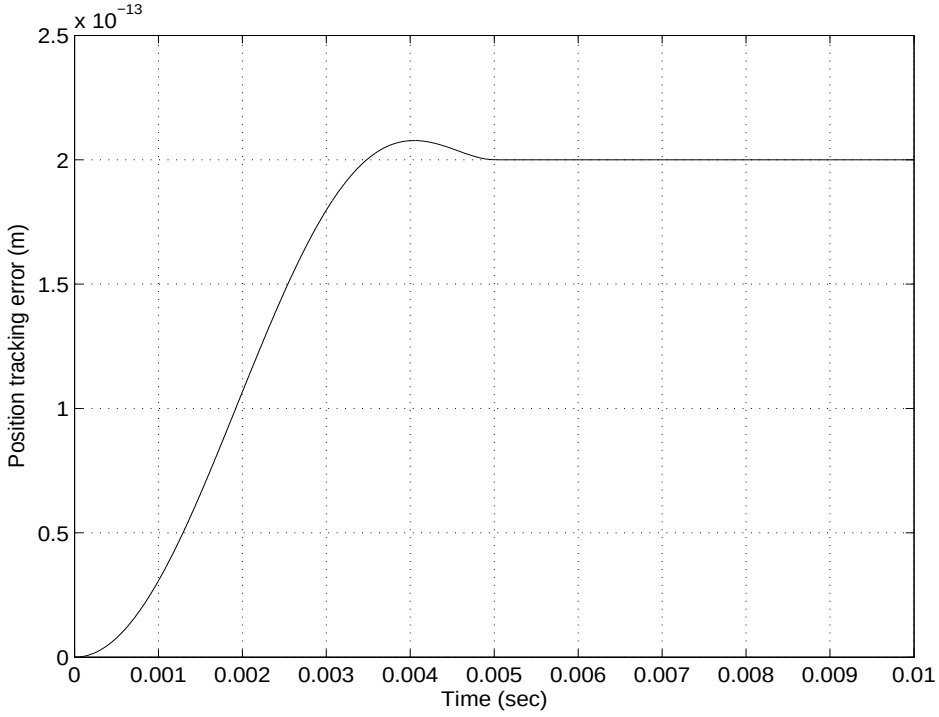

Figure 4.14: *Position tracking error*

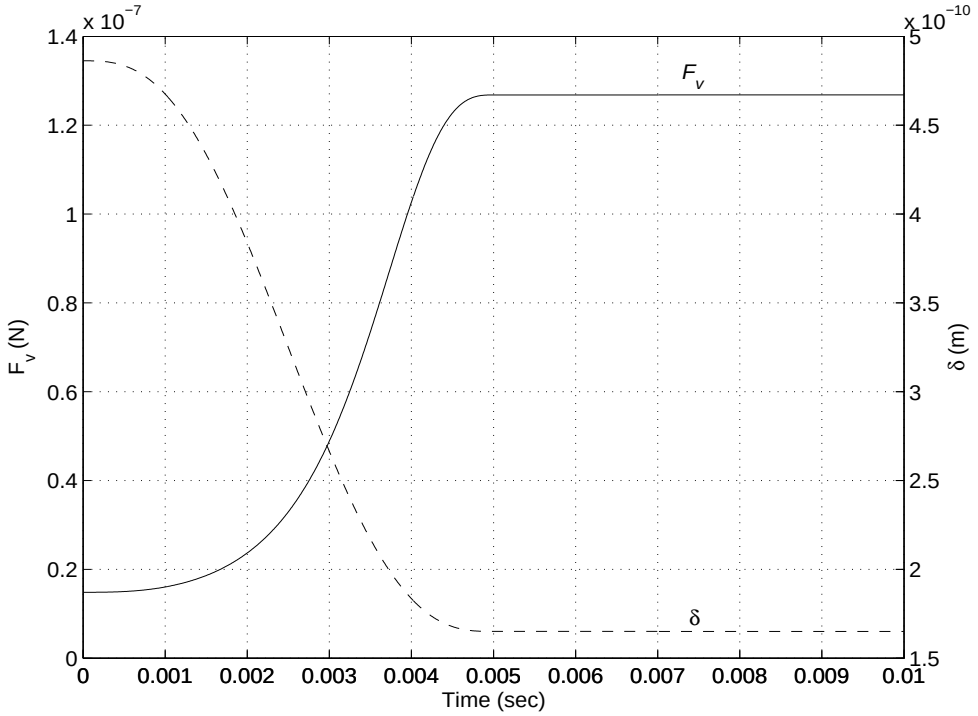

Figure 4.15: *Plot of van der Waals force and δ*

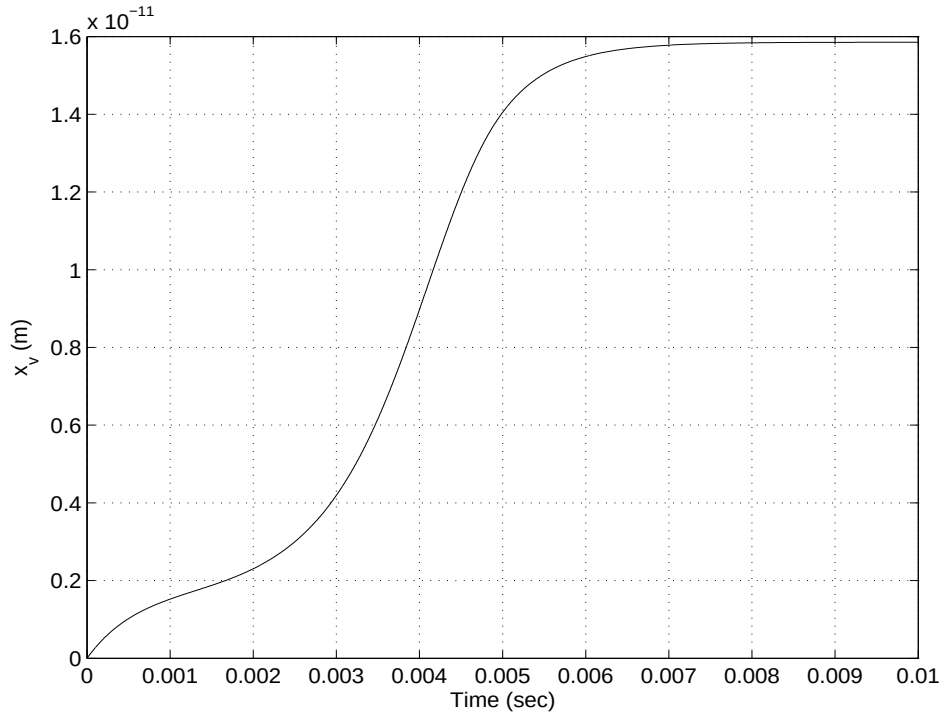

Figure 4.16: *Displacement of piezostack due to van der Waals force*

Chapter 5

PID and Lead-Lag Compensator

In Chapter 4, it has been shown that a simple feedback control gain can not give zero steady state error and good position tracking. Further, the van der Waals force increases the position error. Other control methods are required to get a better result. In this chapter, commonly used linear control laws are designed to control the system.

PID controller and lead-lag compensator are two widely used classical controllers. They are well-known due to their simple implementation. Their basic principles are similar and, sometimes, one of them is referred to the other. Nevertheless, the implementations are different and the result could be discrepant. For a linear system, like the second order system (without van der Waals force) described in Chapter 4, these two control methods are usually able to give satisfactory result. This chapter presents the design of both PID and lead-lag compensators for the system derived in Chapter 4. In the following two sections, the principles and design algorithms of the PID and lead-lag control are briefly described. Simulations are run on the controlled systems and results are discussed.

5.1 PID Control

5.1.1 Introduction

Proportional controller has the effect of reducing the rise time and the steady-state error but does not eliminate it. High proportional gain may destabilize the system. Integral control has the effect of eliminating the steady-state error but it may worsen the transient response. Derivative control increases the stability of the system, reduces the overshoot, and improves the transient response. The combination of corresponding terms in a Proportional-Integral-Derivative (PID) controller is able to provide an acceptable error reduction and satisfactory stability.

In continuous time domain, the ideal PID controller output equation is

$$C(t) = K_P e(t) + K_I \int_0^t e(t^*)dt^* + K_D \frac{de(t)}{dt} \tag{5.1}$$

where K_P, K_I, K_D are the gains for proportional, integral and derivative controls respectively. Increasing K_P and K_I can reduce system errors but may not be able to produce sufficient stability whereas increasing K_D will help to improve stability. The Laplace transform function of Equation (5.1) is

$$C(s) = K_P + \frac{K_I}{s} + K_D s \tag{5.2}$$

Equation (5.2) is the general form for PID control. To design a particular control loop, one has to *tune* the gains in order to achieve the acceptable performance. There are numerous well-developed tuning methods. Some examples are Ziegler-Nichols, Internal Model Control (IMC) and Cohen-Coon. Different methods are used depending on the characteristic of the systems.

5.1.2 Design of the PID Control

There are several forms to express the PID control principle. Sometimes, one form is easier to use than another for a particular design or tuning method. Here, the frequency design method is used to design the PID control. The form preferred is

$$\begin{aligned} C(s) &= \frac{K}{s}\left(T_D s + 1\right)\left(s + \frac{1}{T_I}\right) \\ &= \frac{KT_D}{s}\left(s + \frac{1}{T_D}\right)\left(s + \frac{1}{T_I}\right) \end{aligned} \tag{5.3}$$

$\frac{1}{T_D}$ is the zero of the derivative part of the controller. It is chosen to be placed at the region near the faster pole of the plant. On the other hand, $\frac{1}{T_I}$ is the zero of the integral part. It is usually much smaller than the derivative zero but larger than the slower pole of the plant. With this two zeros and the integral pole, Bode diagram of the open-loop system can be drawn. The last parameter KT_D is then determined so that the phase margin is around 90°. According to the system configuration and motion planning in Chapter 4, the sphere A is moved to 'touch' the other spheres. Thus, overshoot should be prevented as it will cause the spheres to collide so deformation may occur. A phase margin of 90° will ensure very low overshoot.

By using this design method, a PID controller is designed for the system in Chapter 4. The controller parameters obtained are: $\frac{1}{T_D} = -5.87\times10^7$, $\frac{1}{T_I} = -1.59\times 10^3$ and $KT_D = 750$. Equating Equations (5.2) and (5.3) gives the gains for the P, I, D terms in Eq (5.2) as $K_P = 4.4\times10^{10}$, $K_I = 7\times10^{13}$ and $K_D = 750$. However, both Equations (5.2) and (5.3) are hard to implement since the unbound high-frequency gain of the derivative part can lead to a problem. Hence a pole is usually added to the derivative path to limit the gain. Here, a pole $\omega_{pd} = -1 \times 10^4$ is added. The controller equation becomes

$$C(s) = K_p + \frac{K_I}{s} + \frac{K_D s}{1 + s/\omega_{pd}} \tag{5.4}$$

This controller is used for the simulations.

5.1.3 Simulation Results

The PID controller above is employed in the feedback loop of the system. Two inputs are used in the simulations: a step input and the trajectory in Section 4.6. The Simulink model set up for the controlled system with trajectory input is shown in Figure 5.1. Notice that the output x is used to calculate the van der Waals force and then fed back to the plant transfer function. It is to simulate the influence of the van der Waals force on the system. To simulate the step response, the reference input in the model is replaced by the step input and the rest remains the same. The settings of the simulations are

Simulation Parameter	Value
simulation time	0.015 sec
solver option	ode15s
maximum step size	1×10^{-6} sec
relative tolerance	1×10^{-12}

Table 5.1: *Simulation parameters for PID controlled system*

The step response of the controlled system is plotted in Figure 5.2. It shows no overshoot and the settling time is fast, around 1.4×10^{-5}sec. Zero overshoot fulfills the design criteria. For the trajectory input, the position tracking error of the system is shown in Figure 5.3. The collected data shows that the steady state error is about 5.6074×10^{-19}m.

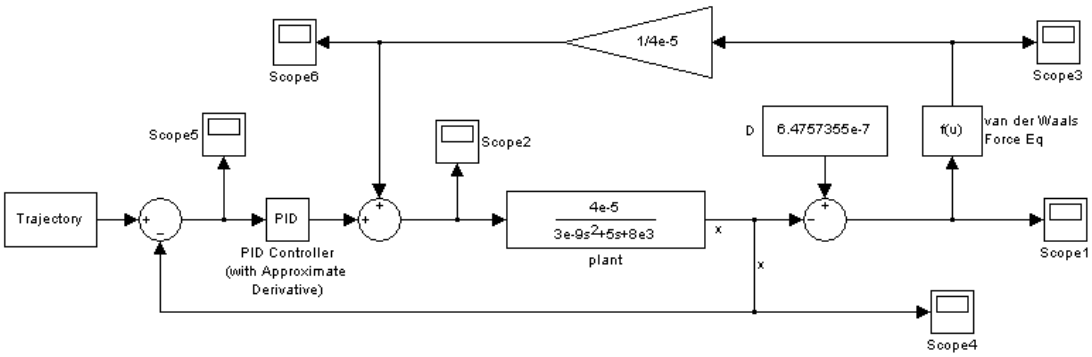

Figure 5.1: *Simulation model for system with PID control*

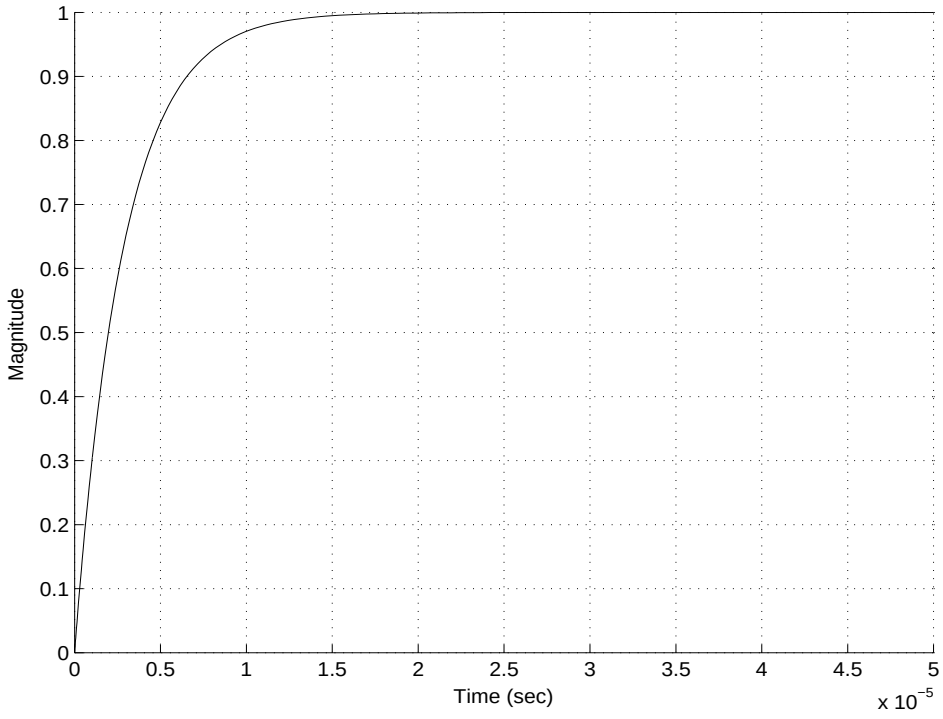

Figure 5.2: *Step response of system with PID control*

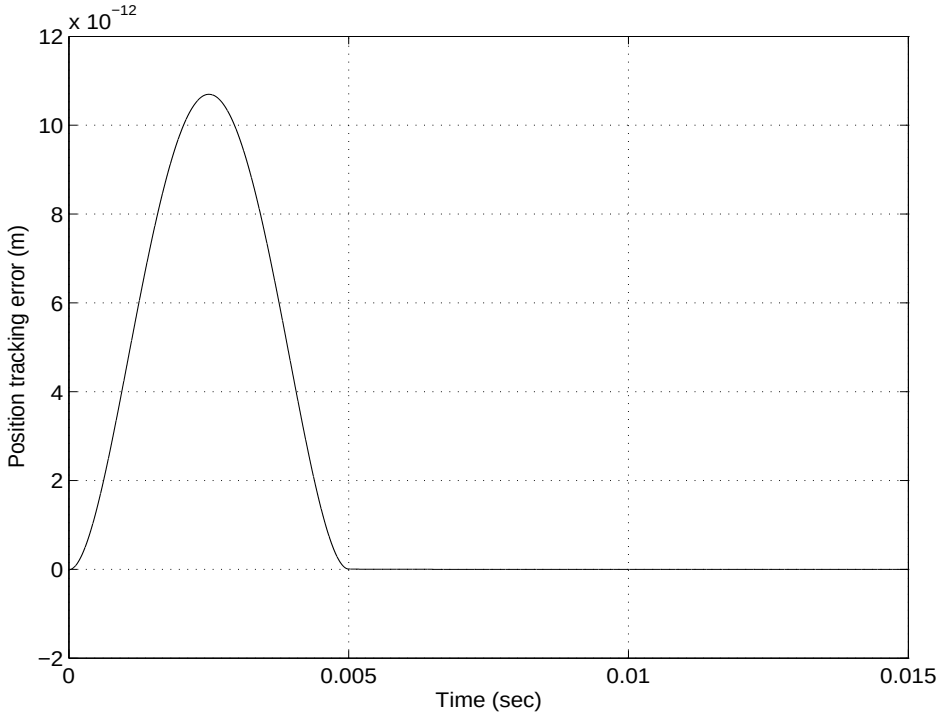

Figure 5.3: *Position tracking error of PID controlled system with trajectory input*

5.2 Lead-Lag Compensator

5.2.1 Introduction

Lead-lag compensation is a conventional control method which has a similar characteristic as PID control. It consists of two parts, lead and lag compensations. Transfer function (5.5) represents both the lead and lag compensations.

$$C(s) = K\frac{(s+z)}{(s+p)} \tag{5.5}$$

It is phase lead when $|z| < |p|$ and phase lag when $|z| > |p|$. K is the control gain. The design of the lead and lag compensations is to select the positions of pole and zero to achieve the specification of the system performance.

The basic principle of the lead compensation is that it adds phase lead near

the crossover frequency to yield desired roots for the closed-loop system. This will increase the system bandwidth and the gain at higher frequencies. If the gain on the low frequency is unchanged, lead compensation will increase the crossover frequency and speed of system response. This characteristic is similar to PD control. Another control which resembles the PI control is the phase lag compensation. The positions of pole and zero are usually at low frequencies that will increase the frequency-response magnitude at low frequency, thus reducing the steady state errors. Lag compensation can be used to obtain the required phase margin by decreasing the frequency-response magnitude at high frequencies. It also has the effect on suppressing high-frequency noise. The combination of the two yields the lead-lag compensation. The overall transfer function is

$$C(s) = K\frac{(s+z_1)(s+z_2)}{(s+p_1)(s+p_2)} \tag{5.6}$$

It possesses the properties of lead and lag compensation. With the right combination of poles and zeros, it is able to improve the system response and lower the steady state error.

5.2.2 Design of Lead-Lag Compensator

There are a few methods to design the lead-lag compensator such as the root locus and frequency design. The frequency design algorithm is briefly described here. Gain K is obtained first, without the compensation, to meet the criteria of phase margin. With the help of the Bode diagram of the open-loop uncompensated system, the crossover frequency is determined and lead compensation is added near the crossover frequency to obtain the required speed of response. Lag compensation is then added to improve the steady state error and response. Finally, gain K is adjusted to improve the overall performance.

Using the design algorithm, the lead-lag compensator transfer function is obtained for the system in Chapter 4 as

$$C(s) = \frac{1\times10^{13}(s+2\times10^{8})(s+1.5\times10^{3})}{(s+1\times10^{9})(s+1)} \tag{5.7}$$

5.2.3 Simulation Results

Simulations were run on the lead-lag compensated system. The Simulink models used are similar to the one used for PID control simulation. The only difference is the block of controller, which is replaced by the zero-pole transfer function representing the lead-lag compensator. Figure 5.4 shows the Simulink model for the system simulation with trajectory input. The settings for the simulations are the same as those in the PID simulation above. Simulation results are given below. Figure 5.5 plots the step response of the controlled system. The settling time of 2.55×10^{-7}sec is faster than the one by PID control. No overshoot is observed and the DC gain is 1. For the trajectory input, Figure 5.6 shows the position tracking error of the system. Comparing to Figure 5.3, the transient response is better, with lower error. However, the steady state error is larger, at about 6.66×10^{-16}m.

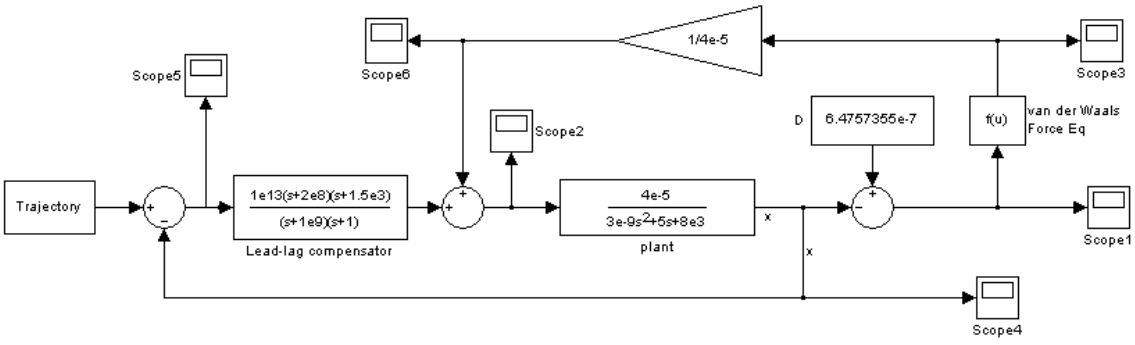

Figure 5.4: *Simulation model for system with lead-lag control*

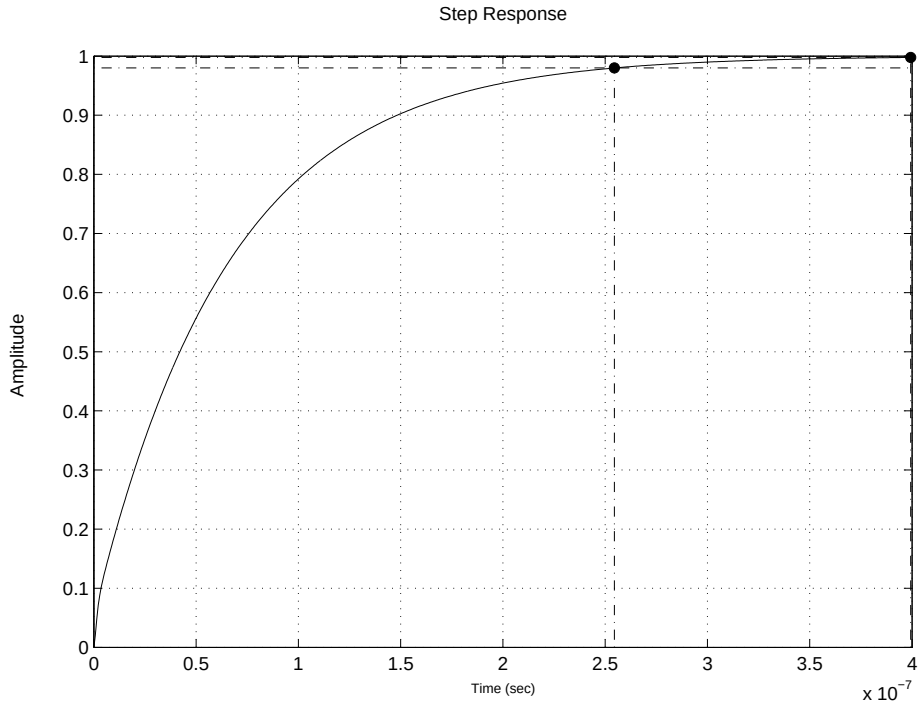

Figure 5.5: *Step response of system with lead-lag control*

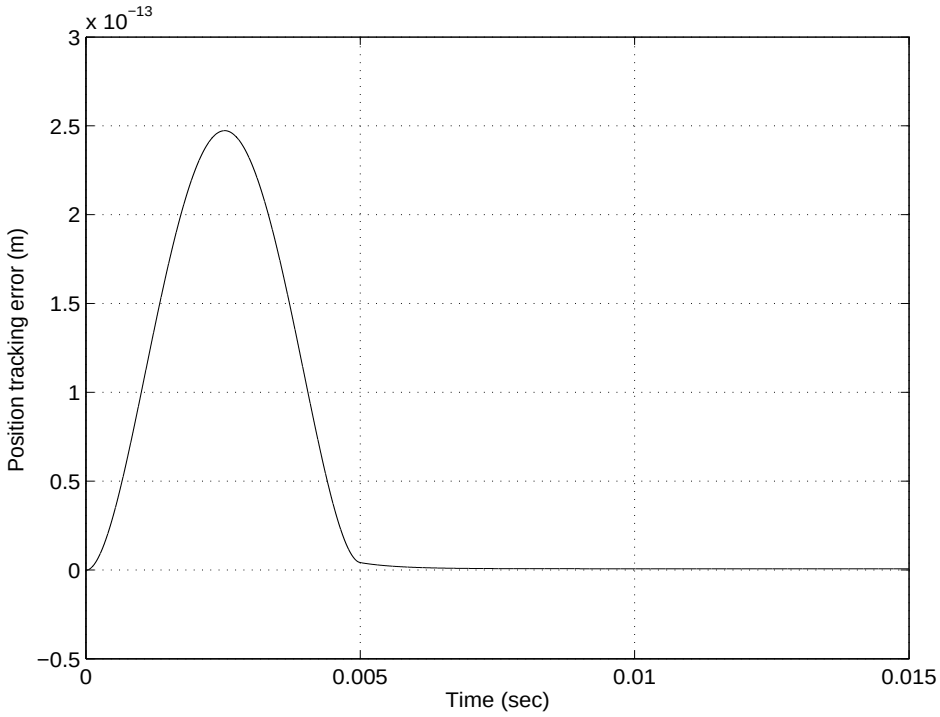

Figure 5.6: *Position tracking error of lead-lag controlled system with trajectory input*

5.3 Discussion

In order to examine the ability of the controllers in attenuating the effect of van der Waals force, two simulation modes are used. One is the controlled systems with van der Waals force input and another is without van der Waals force input. The model with van der Waals force input corresponds to Equation (4.4). The model without van der Waals force also represent the Equation (4.4) but without the van der Waals force formula which is the second term at the right hand side of the equation. Using the two simulation modes, the difference between the system responses with and without van der Waals force under the control of the designed controller can be examined. Taking the PID controlled system for example, Figure 5.1 is the simulation mode with van der Waals force whereas Figure 5.7 shows the simulation mode without van der Waals force. Similarly, lead-lag controlled system is also simulated using these two modes.

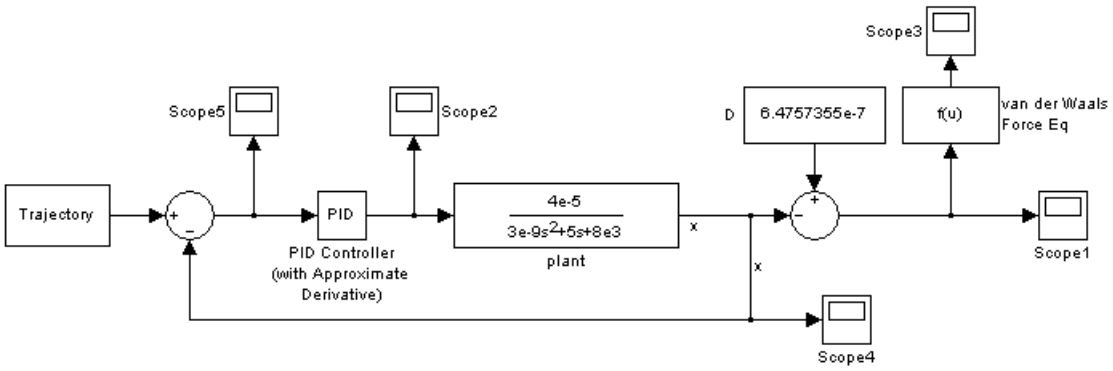

Figure 5.7: *Simulation model for PID controlled system without van der Waals force input*

To see the control effect, the difference of the position tracking errors of the controlled systems with and without van der Waals force inputs are computed. The value of the difference indicates the ability of the controller in attenuating the influence of van der Waals force. The concept is that since the magnitude of

van der Waals force during the motion is very hard to predict especially when the system becomes complicated, a controller which can give low position error of a system does not mean that it can attenuate influence of van der Waals force well. Hence, if we only look at the position tracking error in this system, we may not know if the controllers used can also perform well in other system in terms of reducing the van der Waals force influence. Thus for a general result, we do not solely look at how good the controllers track the position but we compare the position tracking error of the two modes. If the difference is smaller, this means that the position tracking of two simulation modes is similar. The system with van der Waals force model has closer performance to the system without van der Waals force model. In other words, the influence of van der Waals force is less to the controlled system. The smaller the difference value, the better the controller ability to attenuate the influence of van der Waals force. As a result, we know that which and how the controller should be used in micro-system where van der Waals force interacts so that the controller will reduce the influence of van der Waals force.

Figure 5.8 shows difference in position tracking errors for PID and Lead-lag controlled systems. Lead-lag compensation is more efficient in the transient response as the error difference is lower than the PID controlled systems at the first half of the simulation time. However, at steady state, the error difference in PID controlled system is smaller than in the lead-lag compensated system. This indicates that PID control is better attenuating the van der Waals force at the later part of response.

The stability is not properly proven analytically in these two controlled system. It can not be ensured by just observing the simulation results. A theoretical proof is essential. Furthermore, the two linear controls lack robustness in dealing with

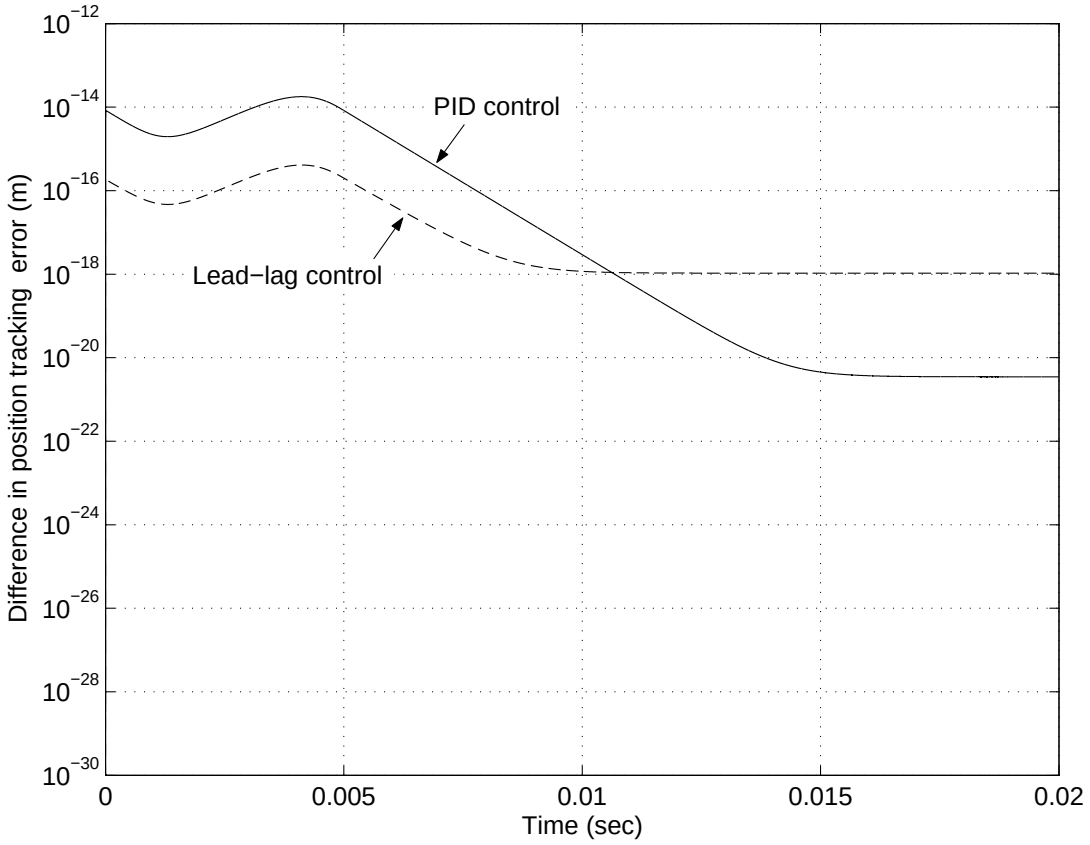

Figure 5.8: *Difference in position tracking error (PID and Lead-lag controlled system)*

the varying van der Waals force. This results in the suboptimal position tracking at transient response. A more complex and robust control method is needed. In next chapter, nonlinear control is investigated to control the system.

Chapter 6

Inverse Dynamics Robust Control

The result in Chapter 5 has shown that linear control, PID and lead-lag control, can not achieve satisfactory result in transient and steady state at the same time. Besides, the robustness and stability issues need to be considered. Since the micromanipulation system with the van der Waals force is a nonlinear system, a nonlinear control law may be used. In this chapter, the inverse dynamics technique is used to control the system. In addition, a robust control method is incorporated in the control law. This will help attenuate the effect of van der Waals force and ensure the stability of the system. The following sections introduce and describe the principles of inverse dynamics robust control. The control law is derived according to the micromanipulation system developed in Chapter 4. In the subsequent section, the parameters of the control law are determined for simulations. Simulation results are presented and discussed at the end.

6.1 Introduction

In robotics, the **inverse dynamics control technique** is widely used to control plants with nonlinear dynamics. The robot's dynamics becomes decoupled and linear. So, efficient techniques from linear control can be used. However, the implementation of this control law requires precise knowledge of the parameters in

the dynamic model of the system. Modelling error and uncertainty in the system may affect the control result. A robust control method is developed to eliminate this problem.

This robust control method assumes the existence of the worst case bound of the modelling error and uncertainty of the system. The bound values are estimated and used in the computation of the control signal. Lyapunov equation is also included as a part of the computation. This will guarantee the stability of the uncertain system. The control signal is nonlinear and could suffer from chattering, which is a characteristic of the discontinuous control law. The principle of the method is described in the next section.

The computed control signal is a modified control signal value which consists of the main control signal for the system model without uncertainty and an additional control signal for the uncertainty. This additional value corrects the system response corresponding to the modelling error and uncertainty. Considering a system with disturbance, if the disturbance is treated as a part of the modelling error or uncertainty of the system, the disturbance should be rejected by using the robust control method. This concept is applied to our micromanipulation system with van der Waals force. If the bound of the van der Waals force can be estimated, the control method is able to attenuate the inaccuracy in the van der Waals force model.

6.2 Inverse Dynamics Robust Control Algorithm

6.2.1 Compensation of the Inverse Dynamics

Controlling compensations for the nonlinear plant dynamics are well-known in robotic, and are described in most books about robot control. The principle is briefly described here. Consider an n-link robot described by the dynamic equation

$$M(\mathbf{q})\ddot{\mathbf{q}} + C(\mathbf{q}, \dot{\mathbf{q}})\dot{\mathbf{q}} + F\dot{\mathbf{q}} + g(\mathbf{q}) = \mathbf{u} \tag{6.1}$$

where $\mathbf{q}$: vector of joint variables

$\mathbf{u}$: control torque vector

$M(\mathbf{q})$: inertia matrix

$C(\mathbf{q}, \dot{\mathbf{q}})\dot{\mathbf{q}}$: coriolis and centrifugal force vector

$F\dot{\mathbf{q}}$: frictional force in system

$g(\mathbf{q})$: gravitational force vector

Setting $H(\mathbf{q}, \dot{\mathbf{q}}) = C(\mathbf{q}, \dot{\mathbf{q}})\dot{\mathbf{q}} + F\dot{\mathbf{q}} + g(\mathbf{q})$, Equation (6.1) becomes

$$M(\mathbf{q})\ddot{\mathbf{q}} + H(\mathbf{q}, \dot{\mathbf{q}}) = \mathbf{u} \tag{6.2}$$

To linearize these dynamics we can use a control law

$$\mathbf{u} = f(\mathbf{q}, \dot{\mathbf{q}}) = M(\mathbf{q})\mathbf{v} + H(\mathbf{q}, \dot{\mathbf{q}}) \tag{6.3}$$

Substituting (6.3) into (6.2) yields

$$\ddot{\mathbf{q}} = \mathbf{v} \tag{6.4}$$

since $M(\mathbf{q})$ is invertible. Equation (6.4) is known as the double integrator system, and is linear and decoupled. It means that the robot links can be controlled independently. Commonly, $\mathbf{v}$ is chosen as

$$\mathbf{v} = \mathbf{r} - K_1\mathbf{q} - K_2\dot{\mathbf{q}} \tag{6.5}$$

where K_1, K_2 are diagonal matrices with diagonal elements consisting of position and velocity gains. They can be chosen as

$$K_1 = diag\{\omega_1^2, \ldots, \omega_n^2\} \tag{6.6}$$
$$K_2 = diag\{2\omega_1, \ldots, 2\omega_n\}$$

where ω is the natural frequency. For a given desired trajectory $\mathbf{q}^d(t), \dot{\mathbf{q}}^d(t)$, $\mathbf{r}$ can be chosen as

$$\mathbf{r}(t) = \ddot{\mathbf{q}}^d(t) + K_2\dot{\mathbf{q}}^d(t) + K_1\mathbf{q}^d(t) \tag{6.7}$$

Substituting (6.7) into (6.5) and defining the tracking error as $\mathbf{e} = \mathbf{q} - \mathbf{q}^d$ gives

$$\mathbf{v} = \ddot{\mathbf{q}}^d - K_1\mathbf{e} - K_2\dot{\mathbf{e}} \tag{6.8}$$

(6.8) is the feedback input to the control law (6.3).

6.2.2 Robust Control

The control algorithm above assumes that the parameters M and H of the system are perfectly modelled. However, modelling error and uncertainty may be present. Hence, instead of (6.3), suppose that the nonlinear control law is actually

$$\mathbf{u} = \hat{M}(\mathbf{q})\mathbf{v} + \hat{H}(\mathbf{q}, \dot{\mathbf{q}}) \tag{6.9}$$

where $\hat{M}, \hat{H}$ are the incorrectly-modelled functions. The uncertainty or modelling error is

$$\Delta M = \hat{M}(\mathbf{q}) - M(\mathbf{q}) \tag{6.10}$$
$$\Delta H = \hat{H}(\mathbf{q}, \dot{\mathbf{q}}) - H(\mathbf{q}, \dot{\mathbf{q}})$$

Equating (6.9) and (6.3) gives

$$M\ddot{\mathbf{q}} + H = \hat{M}\mathbf{v} + \hat{H} \tag{6.11}$$

The arguments are dropped for simplicity. After rearranging the equation, the $\ddot{\mathbf{q}}$ can be expressed as

$$\begin{aligned}\ddot{\mathbf{q}} &= M^{-1}\hat{M}\mathbf{v} + M^{-1}\Delta H \\ &= \mathbf{v} + (M^{-1}\hat{M} - I)\mathbf{v} + M^{-1}\Delta H \\ &= \mathbf{v} + \eta\left(\mathbf{v}, \mathbf{q}, \dot{\mathbf{q}}\right) \end{aligned} \tag{6.12}$$

where $\eta = E(\mathbf{q})\mathbf{v} + M^{-1}\Delta H$ with $E = M^{-1}\hat{M} - I$.

Comparing (6.12) and (6.4), η is the additional input due to the uncertainty or the modelling error of the system. η is unknown but may be estimated. The concept of robust control design is to estimate the 'worst case' bounds on the effects of η on the tracking performance of the system. Then, the control law or input $\mathbf{v}$ is designed to guarantee the stability of the system response and cancel the effect of η as well as possible.

To estimate the worst case bound on η, the following assumptions are made:

(i). $\sup_{t\geq 0} \|\ddot{\mathbf{q}}^d\| < \bar{Q} < \infty$

(ii). $\|E\| = \|M^{-1}\hat{M} - I\| \leq \alpha < 1$ for some α, for all $q \in \mathbb{R}^n$

(iii). $\|\Delta H\| \leq \phi(\mathbf{e}, t)$ for a known function ϕ, bounded in t.

The control law of the robust control is slightly different from (6.8). It is

$$\mathbf{v} = \ddot{\mathbf{q}}^d - K_1\mathbf{e} - K_2\dot{\mathbf{e}} + \Delta\mathbf{v} \tag{6.13}$$

The $\Delta\mathbf{v}$ is the additional feedback term to overcome the effect of uncertainty, η. To compute the control input, the following algorithm is used. Recall that the tracking error is defined as

$$\mathbf{e} = \mathbf{q} - \mathbf{q}^d \tag{6.14}$$

$$\therefore \quad \dot{\mathbf{e}} = \dot{\mathbf{q}} - \dot{\mathbf{q}}^d \tag{6.15}$$

Then, to form a state space equation,

$$\dot{\mathbf{e}}_\mathbf{1} = \mathbf{e_2} \tag{6.16}$$

$$\begin{aligned}\dot{\mathbf{e}}_\mathbf{2} &= \ddot{\mathbf{q}} - \ddot{\mathbf{q}}^d \\ &= \ddot{\mathbf{q}} - \mathbf{v} - K_1\mathbf{e} - K_2\dot{\mathbf{e}} + \Delta\mathbf{v} \\ &= \eta - K_1\mathbf{e_1} - K_2\mathbf{e_2} + \Delta\mathbf{v}\end{aligned} \tag{6.17}$$

Thus,

$$\begin{bmatrix}\dot{\mathbf{e}}_\mathbf{1} \\ \dot{\mathbf{e}}_\mathbf{2}\end{bmatrix} = \begin{bmatrix}0 & I \\ 0 & 0\end{bmatrix}\begin{bmatrix}\mathbf{e_1} \\ \mathbf{e_2}\end{bmatrix} + \begin{bmatrix}0 \\ I\end{bmatrix}\left(-\begin{bmatrix}K_1 & K_2\end{bmatrix}\begin{bmatrix}\mathbf{e_1} \\ \mathbf{e_2}\end{bmatrix} + \Delta\mathbf{v} + \eta\right) \tag{6.18}$$

With $K = [K_1 \quad K_2]$ and $\mathbf{e} = [\mathbf{e_1}, \mathbf{e_2}]$, and let

$$A = \begin{bmatrix}0 & I \\ 0 & 0\end{bmatrix} \quad B = \begin{bmatrix}0 \\ I\end{bmatrix}$$

The equation becomes

$$\begin{aligned}\dot{\mathbf{e}} &= A\,\mathbf{e} + B(-K\mathbf{e} + \Delta\mathbf{v} + \eta) \\ &= (A - BK)\mathbf{e} + B(\Delta\mathbf{v} + \eta) \\ &= \bar{A}\,\mathbf{e} + B(\Delta\mathbf{v} + \eta)\end{aligned} \tag{6.19}$$

where $\bar{A} = (A - BK)$. With the control input $\mathbf{v}$ as given in (6.13), we have,

$$\begin{aligned}\eta &= E(\mathbf{q})\mathbf{v} + M^{-1}\Delta H \\ &= E(\ddot{\mathbf{q}} - K\mathbf{e} + \Delta\mathbf{v}) + M^{-1}\Delta H \\ &= E\Delta\mathbf{v} + E(\ddot{\mathbf{q}} - K\mathbf{e}) + M^{-1}\Delta H\end{aligned} \tag{6.20}$$

For the system (6.19), suppose that there exists a continuous function $\rho(\mathbf{e}, t)$ which is bounded in time t and satisfies the inequalities

$$\|\Delta\mathbf{v}\| < \rho(\mathbf{e}, t) \tag{6.21}$$

$$\|\eta\| < \rho(\mathbf{e}, t) \tag{6.22}$$

Using the assumptions 1-3 above and (6.21) and (6.22), the function ρ can be determined as follows.

$$\begin{aligned} \|\eta\| &\leq \|E\Delta\mathbf{v} + E(\ddot{\mathbf{q}}^d - K\mathbf{e}) + M^{-1}\Delta H\| \\ &\leq \alpha\rho(\mathbf{e},t) + \alpha(\bar{Q} + \|K\| \cdot \|\mathbf{e}\|) + \overline{M}\phi(\mathbf{e},t) \\ &= \rho(\mathbf{e},t) \end{aligned} \tag{6.23}$$

where $\overline{M}$ is the upper bound of $\|M^{-1}\|$. From this, ρ can be solved as

$$\rho(\mathbf{e},t) = \frac{1}{1-\alpha}\Big(\alpha\bar{Q} + \alpha\|K\| \cdot \|\mathbf{e}\| + \overline{M}\phi(\mathbf{e},t)\Big) \tag{6.24}$$

To ensure stability, choose a symmetric, positive definite matrix Q and let P be the unique positive definite symmetric solution to the Lyapunov equation

$$\bar{A}^T P + P\bar{A} + Q = 0 \tag{6.25}$$

Finally, the additional feedback input can be calculated as

$$\Delta\mathbf{v} = \begin{cases} -\rho(\mathbf{e},t)\dfrac{B^T P\mathbf{e}}{\|B^T P\mathbf{e}\|} & \text{if} \quad \|B^T P\mathbf{e}\| \neq 0 \\ 0 & \text{if} \quad \|B^T P\mathbf{e}\| = 0 \end{cases} \tag{6.26}$$

To summarize, the robust control law for the system (6.2) is

$$\mathbf{u} = M(\mathbf{q})(\mathbf{v} + \boldsymbol{\Delta}\mathbf{v}) + H(\mathbf{q}, \dot{\mathbf{q}}) \tag{6.27}$$

where $\mathbf{v}$ is the feedback input as (6.8) in the inverse dynamics control, which is the major control input for the system. $\boldsymbol{\Delta}\mathbf{v}$ is the additional feedback input (6.26) derived from robust control that eliminates the effect of uncertainty or modelling error. More details of the robust control can be found in [37].

6.3 Derivation of Control Law for the Micromanipulation System

The inverse dynamics robust control method above is also suitable for the micromanipulation system developed in Chapter 4. The following describes the

derivation of the robust control law.

From (4.4), with the control signal $u = k_p\, d_{33}\, NV$, we obtain the dynamic model of the system with van der Waals force as

$$M\ddot{x} + c\dot{x} + k_p x = u + \frac{64AR^6(D-x)}{3\left[(D-x)^2 + l^2 - 4R^2\right]^2\left[(D-x)^2 + l^2\right]^2} \tag{6.28}$$

Let $F_v(x)$ be the van der Waals force formula. Moving this to the left hand side, the equation becomes

$$M\ddot{x} + c\dot{x} + k_p x - F_v(x) = u \tag{6.29}$$

This is the actual dynamic equation of the system. However, if the van der Waals force formula is not known, the model of the dynamic equation becomes incorrect and the problem of modelling error or uncertainty occurs. Hence, the robust control law must be included. For the system, the control law is chosen to be

$$u = M(v + \Delta v) + c\dot{x} + k_p x \tag{6.30}$$

The tracking errors are defined as

$$e_1 = x - x_d \tag{6.31}$$

$$e_2 = \dot{x} - \dot{x}_d \tag{6.32}$$

where x_d is the desired position. Then,

$$\dot{e}_1 = e_2 \tag{6.33}$$

$$\begin{aligned}
\dot{e}_2 &= \ddot{x} - \ddot{x}_d \\
&= \frac{u}{M} + \frac{F_v(x)}{M} - \frac{c}{M}\dot{x} - \frac{k_p}{M}x - \ddot{x}_d \\
&= \frac{M(v+\Delta v) + c\dot{x} + k_p x}{M} + \frac{F_v(x)}{M} - \frac{c}{M}\dot{x} - \frac{k_p}{M}x - \ddot{x}_d \\
&= (v + \Delta v) + \frac{F_v(x)}{M} - \ddot{x}_d
\end{aligned} \tag{6.34}$$

Choose $v = \ddot{x}_d - K_1 e_1 - K_2 e_2$, then

$$\dot{e}_2 = -K_1 e_1 - K_2 e_2 + \Delta v + \frac{F_v(x)}{M} \tag{6.35}$$

The state space equation can be written as

$$\begin{bmatrix} \dot{e}_1 \\ \dot{e}_2 \end{bmatrix} = \begin{bmatrix} 0 & 1 \\ -K_1 & -K_2 \end{bmatrix} \begin{bmatrix} e_1 \\ e_2 \end{bmatrix} + \begin{bmatrix} 0 \\ 1 \end{bmatrix} (\Delta v + \eta) \tag{6.36}$$

$$\dot{\mathbf{e}} = A\mathbf{e} + B(\Delta v + \eta) \tag{6.37}$$

where

$$A = \begin{bmatrix} 0 & 1 \\ 0 & 0 \end{bmatrix} \quad B = \begin{bmatrix} 0 \\ 1 \end{bmatrix} \quad \eta = \frac{F_v(x)}{M} \tag{6.38}$$

In the derivation, it is assumed that the only uncertainty is the van der Waals force. Since M is a constant and $F_v(x)$ is a bounded value,

$$\|\eta\| \leq \frac{\|F_v(x)\|_{max}}{M} = \rho \tag{6.39}$$

where $\|F_v(x)\|_{max}$ is the 'worst case' bound of $F_v(x)$. The Lyapunov equation is then solved for P, by letting $Q = I$,

$$A^T P + PA + I = 0$$

After that, Δv is obtained as

$$\Delta v = \begin{cases} -\rho(\mathbf{e}, t)\dfrac{B^T P\mathbf{e}}{\|B^T P\mathbf{e}\|} & \text{if} \quad \|B^T P\mathbf{e}\| \neq 0 \\ 0 & \text{if} \quad \|B^T P\mathbf{e}\| = 0 \end{cases} \tag{6.40}$$

6.4 Simulations

6.4.1 Control Parameters

Having derived the control law for the micromanipulation system, the parameters are determined as follows.

Designed gains: $K_1 = 1\times10^{18}, K_2 = 1\times10^{6}$.

$$A = \begin{bmatrix} 0 & 1 \\ -1\times10^{18} & -1\times10^{6} \end{bmatrix} \quad B = \begin{bmatrix} 0 \\ 1 \end{bmatrix} \tag{6.41}$$

Solving the Lyapunov equation gives

$$P = \begin{bmatrix} 5\times10^{11} & -1.25\times10^{-19} \\ -1.25\times10^{-19} & 5\times10^{-7} \end{bmatrix} \tag{6.42}$$

Then,

$$B^T P\mathbf{e} = -1.25\times10^{-19}e_1 + 5\times10^{-7}e_2 \tag{6.43}$$

$$\|B^T P\mathbf{e}\| = \sqrt{(-1.25\times10^{-19}e_1)^2 + (5\times10^{-7}e_2)^2} \tag{6.44}$$

The 'worst case' bound of van der Waals force is calculated using Eq. (4.3). Substituting the parameters from Table 4.5, $D = 6.47573557\times10^{-7}$m from Section 4.6 and $x = 1\times10^{-8}$m, the final position which will give the maximum value for the van der Waals force, we get $\|F_v(x)\|_{max} = 1.2685\times10^{-7}$N. So,

$$\frac{\|F_v(x)\|_{max}}{M} = 42.2833 = \rho \tag{6.45}$$

Thus, the additional feedback is obtained as

$$\Delta v = \begin{cases} -42.2833\dfrac{B^T P\mathbf{e}}{\|B^T P\mathbf{e}\|} & \text{if} \quad \|B^T P\mathbf{e}\| \neq 0 \\ 0 & \text{if} \quad \|B^T P\mathbf{e}\| = 0 \end{cases} \tag{6.46}$$

Recall that the desired trajectory is $x_d = 0.0012t^2 - 0.16t^3$ which gives

$$\dot{x}_d = 0.0024t - 0.48t^2, \quad \text{desired velocity} \tag{6.47}$$

$$\ddot{x}_d = 0.0024 - 0.96t, \quad \text{desired acceleration} \tag{6.48}$$

With the definitions of (6.31) and (6.32), and the system parameters obtained in Section 4.4, the control law for the micromanipulation system is

$$u = 3\times10^9(v + \Delta v) + 5\dot{x}_d + 8000x_d \tag{6.49}$$

where $v = \ddot{x}_d - 1\times10^{18}e_1 - 1\times10^6 e_2$ and Δv as in (6.46).

6.4.2 Results

Figure 6.1 shows the Simulink model used for inverse dynamics robust control of the system. Notice that there are two subsystem models in the figure, namely the controller and the plant which are shown in Figures 6.2 and 6.3 respectively. The 'S-Function' block is the calculating function for Δv (Eq. 6.46). The settings of the simulations are

Simulation Parameter	Value
simulation time	0.015 sec
solver option	ode23tb
maximum step size	2×10^{-6} sec
relative tolerance	auto

Table 6.1: *Simulation parameters for inverse dynamics robust control system*

Due to the complexity of the calculation, the solver option employed is ode23tb. This is a stiff problem solver suitable for this problem.

Simulation results of the system with the robust control law are shown in Figure 6.4. The position tracking error is smaller than the order of 10^{-16}m throughout the motion. The transient response is better than the PID and Lead-lag controlled system. The steady state error is very low, about 1.3483×10^{-21}m. It is smaller than the result by the PID and Lead-lag controls, which means that the position tracking ability of this robust control is very well. The control signal required is shown in Figure 6.5. The effort (voltage) needed is small and easy to obtain. Figure 6.6 shows the magnitude of the difference in position tracking error. The overall values are smaller than those in systems with PID and Lead-lag controls. At steady state, the values are of the order 10^{-21}m. The small values indicate that the inverse dynamics robust controller is effective at reducing the effect of van der

Waals force on the system. Thanks to the nonlinear control term Δv, it provides the ability to eliminate the van der Waals force effect. With the term, the position tracking is improved.

6.5 Discussion

Robustness is an important capability of this control algorithm. It is not only shown by the low position tracking error, but also can be seen from the transient response where the tracking error is very small. Compared to the result of PID and Lead-lag control, it can deal better with the varying van der Waals force throughout the motion. In this robust control method, stability is ensured by the Lyapunov equation. Since the Lyapunov stability test is included as a part of the design procedure, if a control law is derived successfully, the result is guaranteed to be stable. This is not given in either the PID or Lead-lag control.

One difference between the inverse dynamics robust control and the linear control methods is the van der Waals force involved in the design. In linear control, the system is assumed to be without van der Waals force so that the system is linear and the control procedure can be carried out. After getting the control gains, the van der Waals force is added in the system for analysis. However, in the nonlinear control approach, the van der Waals force is treated as a part of control law. Although the van der Waals force formula is not used explicitly, it is modelled as an uncertainty term in the control law. The estimated upper bound helps the derivation of the extra control term which is used to cancel the van der Waals force. The result shows that this method does improve the position tracking error and reduces the influence of van der Waals force. There is no chattering problem occurring in the control. It is probably because of the simple structure of the model.

In short, compared to the linear controls, the inverse dynamics robust control gives better system response and low position tracking error. It is also effective at reducing the van der Waals force effect on the system. Nevertheless, this method may be harder to implement due to the existence of the nonlinear Δv. The nonlinear equation may cause discontinuity in the control signal that can result in application problems. This problem should be taken care of when it is applied to the hardware.

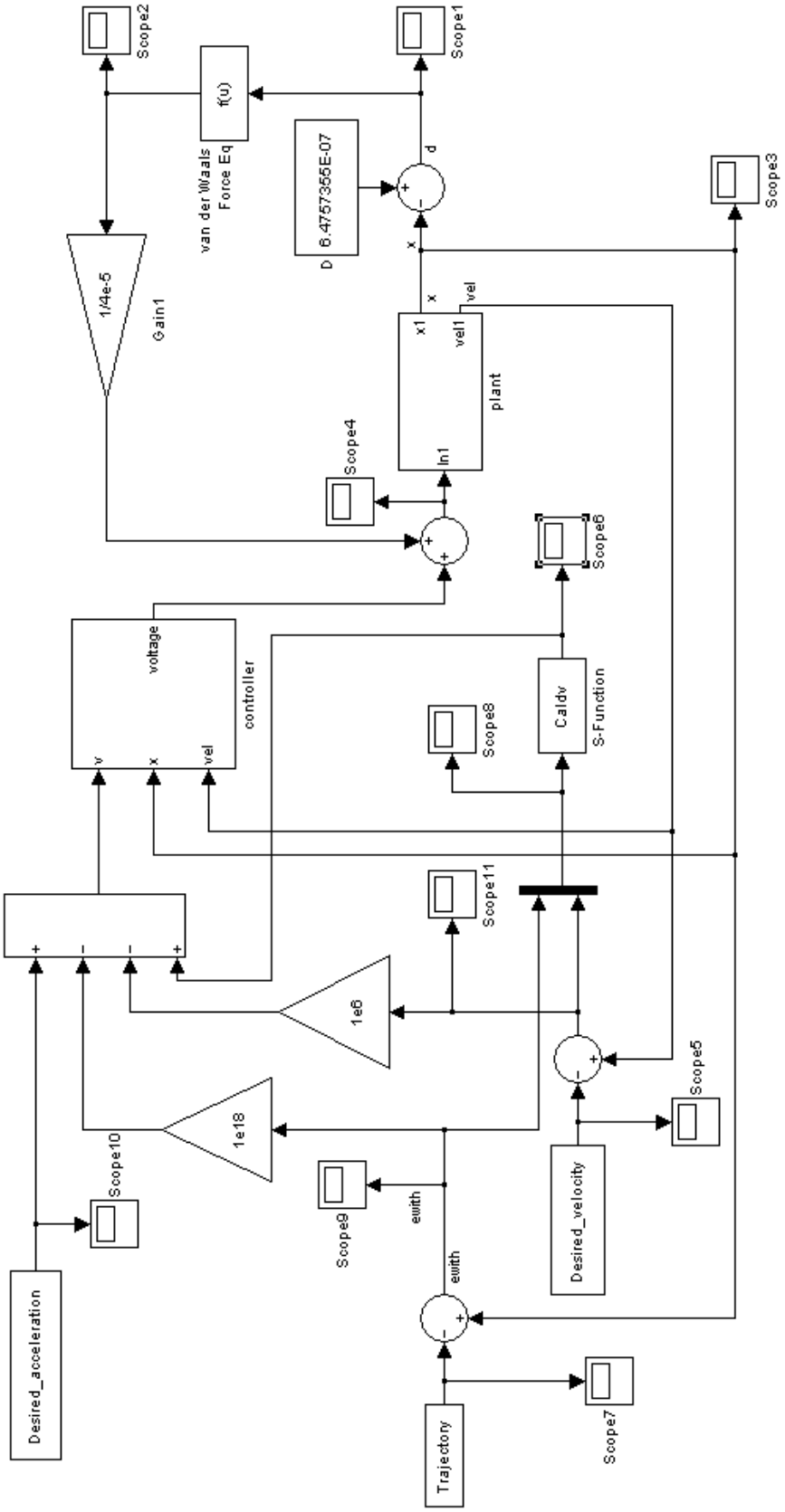

Figure 6.1: *Simulation model of inverse dynamics robust control system*

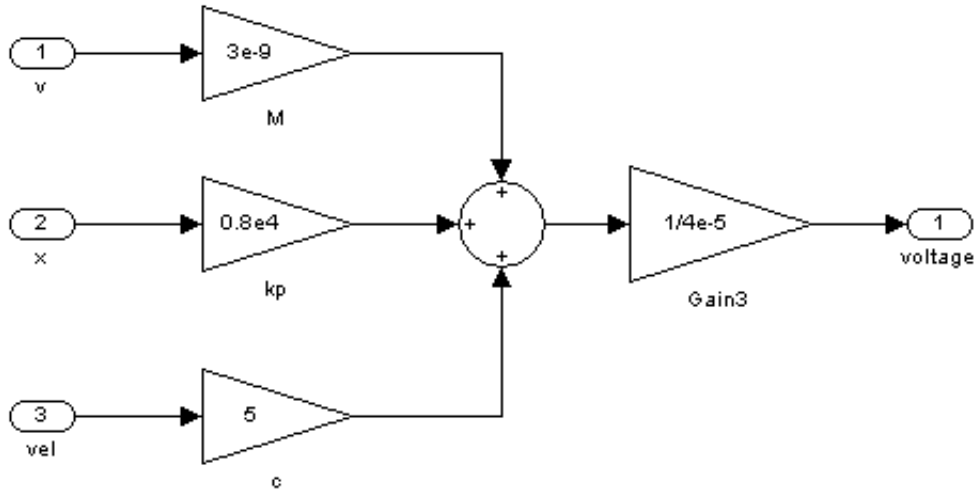

Figure 6.2: *Simulation model of control subsystem*

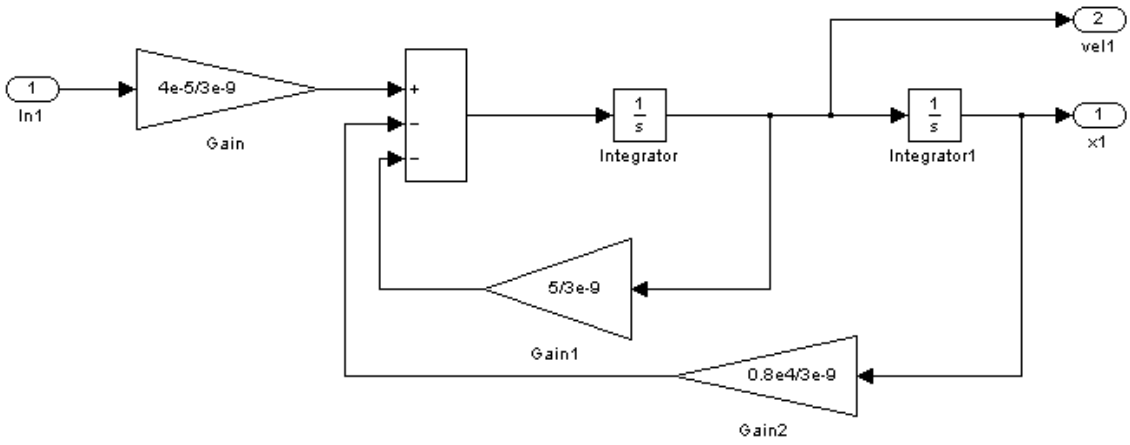

Figure 6.3: *Simulation model of plant subsystem*

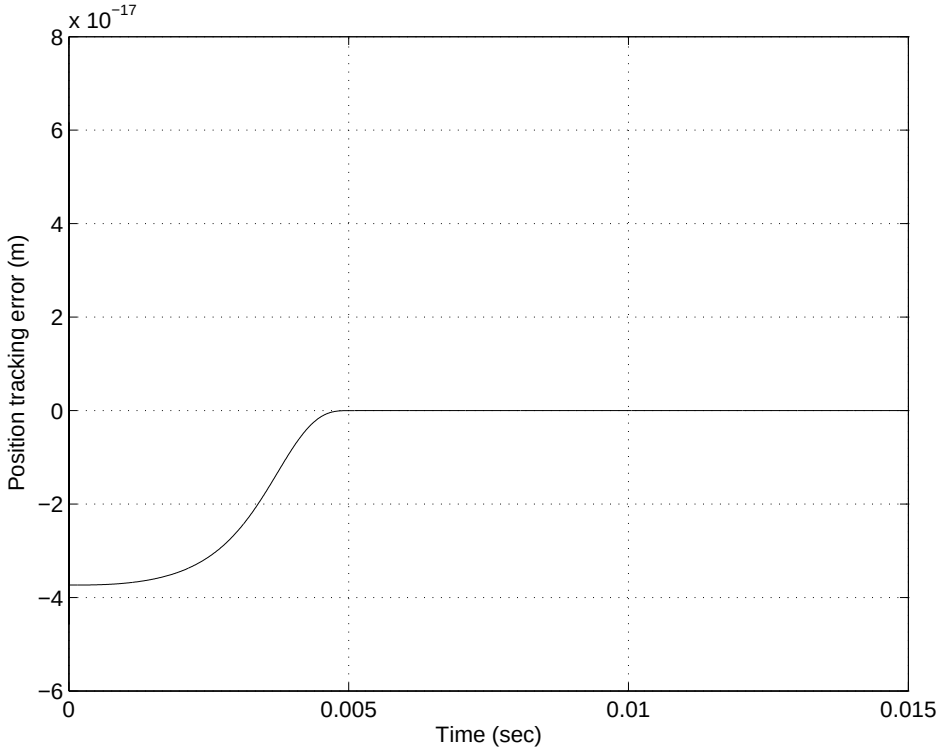

Figure 6.4: *Position tracking error of inverse dynamics robust controlled system with trajectory input*

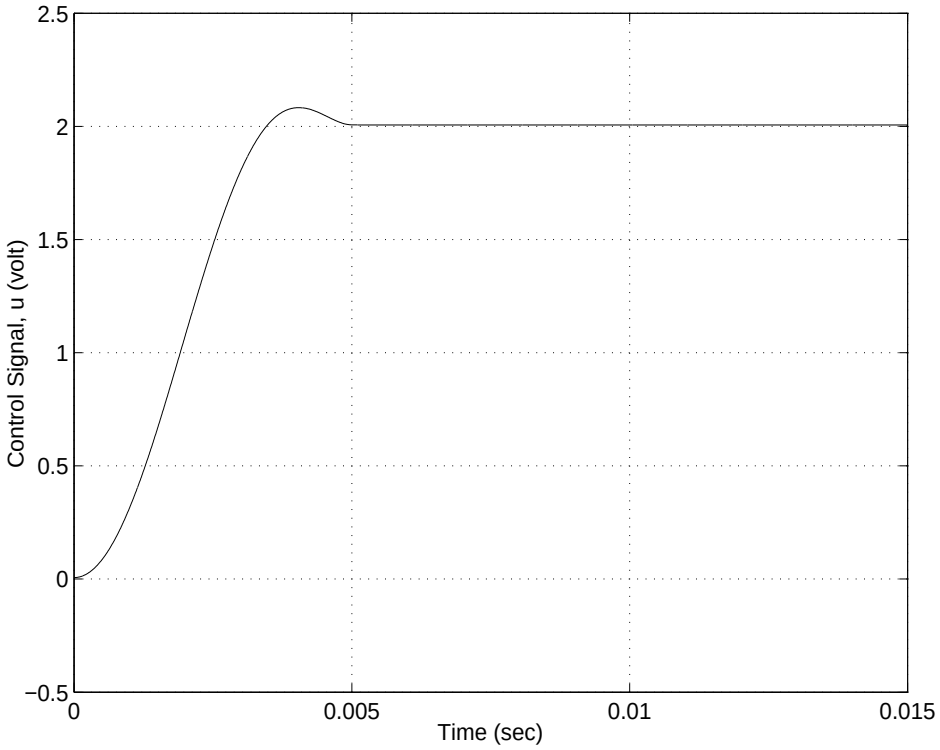

Figure 6.5: *Control signal sent to the system plant, u*

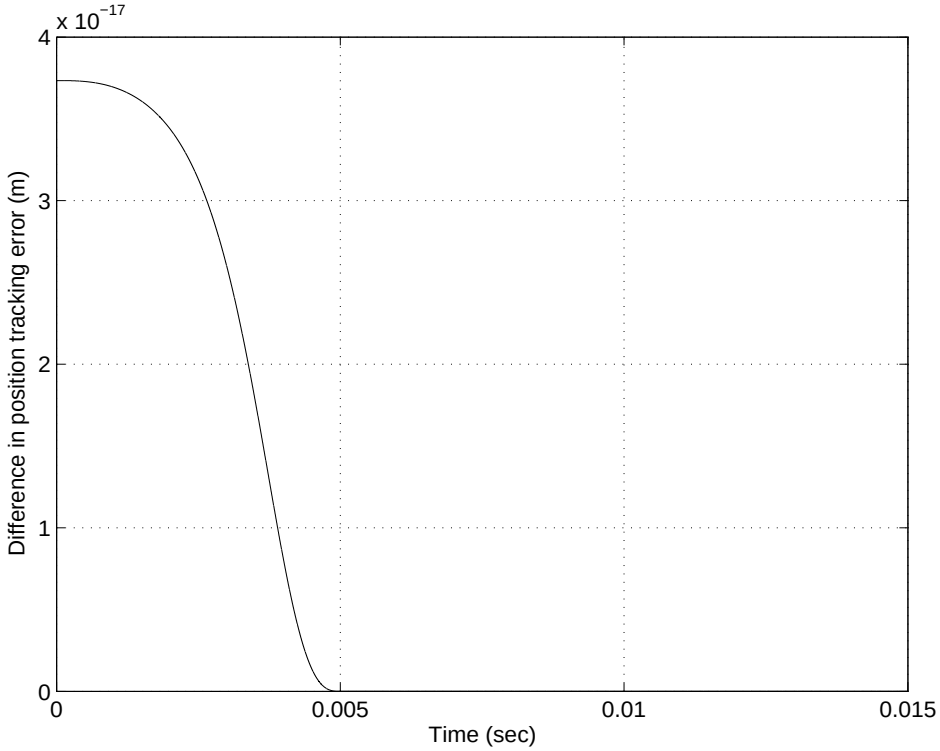

Figure 6.6: *Difference in position tracking error (inverse dynamics robust control system)*

Chapter 7

Conclusions

This thesis has investigated various control approaches on a micromanipulation system under the influence of van der Waals force. It also examined the ability of the control laws in attenuating the effect of van der Waals force on the system. A micromanipulation system which exhibits the significant effect of van der Waals force has been modelled for simulation. Results of simulations using three distinct control laws – PID control, lead-lag compensator and inverse dynamics robust control were examined. The task of the system was to move an object from an initial distance to 'touch' another object. With a planned trajectory, the simulation has shown that van der Waals force changes with the system motion, and the position tracking error becomes significant due to this force.

7.1 Control Issue

PID and lead-lag compensator are designed to control the system. Two simulation modes, with van der Waals force input and without van der Waals force input, are run to investigate the controller performance. The difference between the position tracking errors shows the effectiveness of the controller in attenuating the van der Waals force effect. The result shows that the PID controller is better in

attenuating the force effect in steady state whereas the lead-lag compensator is good at the transient response.

Since the dynamics of the manipulation system with van der Waals force is nonlinear, a nonlinear control is considered. The system is treated as a single degree freedom robotic system. The inverse dynamics robust control law is derived which takes into account the van der Waals force and consider realistic parameter values. The simulation results show that the position tracking error is very low. The difference of the position tracking errors between the two simulation modes is smaller than the value by lead-lag compensator. When compared to PID, it is lower in transient response but larger in steady state. Nevertheless, the values are kept at a very low amount, at the order of 10^{-21} which is acceptable. In general, this nonlinear control law is effective in attenuating the effect of van der Waals force and it is able to give very low tracking error. Furthermore, the Lyapunov equation in the robust control is able to ensure the stability of the system response. Another advantage is the robustness of the control law which gives the ability to cope with the varying van der Waals force. In designing the robust control, van der Waals force is modelled as an uncertainty which is used to derived the additional control signal. With this extra control, the results show that the control is better in dealing with the van der Waals force.

Although the result of the inverse dynamics robust control is better in overall compared to the PID and lead-lag control, one problem remained is the real-time computation of the control signal. The control signal of the robust control law may be chattering and discontinuous since it consists of a nonlinear equation for Δv (Eq 6.26). This makes its implementation harder than PID and lead-lag control. Hence, to obtain a good practical result, removing the chattering of control signal

should be the next step and this could be a future research subject.

7.2 Contributions

This thesis helps to lay out the foundation for understanding the influence of van der Waals force on micromanipulation system and control effect on the system with the interference of the van der Waals force. It pointed out that the existence of the van der Waals force can disturb the position tracking of the system. It also shows that if the van der Waals force is considered in the control law, the control law has a better ability in attenuating the effect of van der Waals force on the system. This has been shown in the inverse dynamics robust control. The control also help in improving the accuracy of position tracking in micromanipulation system.

The simulation of the long range effect of microscopic force on micromanipulation system can be a reference for future design. It can be used for other micro-system such as system with different task and multiple degree of freedom. The control law derived in the Chapter 6 provides a new aspect in controlling the micromanipulation system. Continuing from the control law, more advanced control method may be developed.

7.3 Future Research Possibilities

(i). **Considering other microscopic force**. This project only considers the van der Waals force and assuming other microscopic forces are insignificant. However, when the working environment condition is not perfect, such as if the humidity is not zero, other force like surface tension and electrostatic forces may present and involve in the system. Further investigation may be

carried out on the effect of other microscopic forces on the micromanipulation system.

(ii). **Experimental work**. The work in the thesis may be put into practical experiments. The experimental results can then be compared with the simulation results. Thus, the validity of the simulation results can be checked. Also, further possible problem of the work in the thesis and micromanipulation may be observed.

(iii). **Considering other system setting**. In this thesis, a simple one degree of freedom system is used. Multiple degree of freedom may be developed for investigation. Besides, other task of system other than transferring objects may be considered such as retreating objects from a pile, pushing an object passing others, etc.

Bibliography

[1] Yamamoto, T., O. Kurosawa, H. Kabata, N. Shimamoto and M, Washizu, Molecular Surgery of DNA based on Electrastatics Micromanipulation, IEEE Transaction on Industry Applications, Vol. 36, No. 4, 2000, pp. 1010-1017.

[2] Arai, F., D. Andou, Y.Nonoda, T. Fukuda and T. Oota, Micro Manipulation Based on Micro Physics - Stratey Based on Attractive Force Reduction and Stress Measurement, Proc. 1995 Int. Conf. on Robotics and Automation, pp. 236-241.

[3] Fearing R.S., Survey of Sticking Effects of Micro Parts Handling, Proceedings of the International Conference on Intelligent Robots and Systems, 1995 IEEE, pp. 212-217.

[4] Sitti, M. and H. Hashimoto, Force Controlled Pushing of Nanoparticles: Modeling and Experiments, Proc. 1999 IEEE/ASME Int. Conf. on Advanced Intelligent Mechatronics, September 1999, Atlande, USA, pp. 13-20.

[5] Feddema, J.T., Xavier, P. and Brown, R. Micro-Assembly Planning with van der Waals Force, Proc. of the 1999 IEEE International Symposium on Assembly and Task Planning, July 1999, Porto, Portugal, pp. 32-38.

[6] Arai, F., D. Andou, Y.Nonoda, T. Fukuda, H. Iwata and K. Itoigawa, Integrated Microendeffector for Micromanipuplation, IEEE/ASME Transactioins on Mechatronics, Vol. 3, No. 1, march 1998, pp. 17-23.

[7] Zhou, Y. and B.J. Nelson, Force Controlled Microgripping, Microrobotics and Microassembly - Proceedings of SPIE, Vol. 3834, 1999, pp. 211-221.

[8] Rollot, Y., S. Régnier and J.-C. Guinot, Simulation of micro-manipulations: Adhesion forces and specific dynamic models, International Journal of Adhesion and Adhesives, 19, 1999, pp. 35-48.

[9] Zhou, Y., B.J. Nelson and B. Vikramaditya, Fusing Force and Vision Feedback for Micromanipulation, Proc. 1998 IEEE Int. Conf. on Robotics and Automation, May 1998, Leuven, Belgium, pp. 1220-1225.

[10] Arai, F., Y. Nonoda, T. Fukuda and T. Oota, New Force Measurement and Micro Grasping Method Using Laser Raman Spectrophotometer, Proc. 1996 IEEE Int. Conf. on Robotics and Automation, April 1996, Minneapolis, Minnesota, pp. 2220-2225.

[11] Kimura, M. and M. Fujiyashi, Force Measurement and Control of Electrostatic Micro-actuator, Proceedings of 2nd International Symposium on Micro Machine and Human Science, 1991, pp. 119-124.

[12] Kobayashi, H. and S. Iijima, Micro Robotic Manipulator, Proceedings of 2nd International Symposium on Micro Machine and Human Science, 1991, pp. 125-132.

[13] Zhang, Z., M.A. Ferenczi, A.C. Lush and C.R. Thomas, A Novel Micromanipulation Technique for Measuring the Bursting Strength of Single Mammalian Cells, Applied Microbiology and Biotechnology, 36, pp. 208-210, 1991.

[14] Zhang, Z., M.A. Ferenczi and C.R. Thomas, A Micromanipulation Technique with a Theoretical Cell Model for Determining Mechanical Properties of Single Mammalian Cells, Chemical Engineering Science, Vol. 47, No. 6, pp. 1347-1354, 1992.

[15] Zhang, Z., C.R. Thomas and C. Cowen, Micromanipulation Measurements of Biological Materials, Biotechnology Letters, 22, pp. 531-537, 2000.

[16] Fahlbusch, S. and S. Fatikow, Force Sensing in Microrobotic Systems - An Overview, Proc. of 5th IEEE Int. Conf. on Electronics, Circuits and Systems, 7-10 September 1998, Lisboa, Portugal, pp. 259-262.

[17] Bellouard, Y., R. Clavel, R. Gotthardt, J.-E. Bidaux and T. Sidler, A New Concept of Monolithic Shape Memory Alloy Micro-devices Used in Microrobotics, Actuator '98 - 6th Int. Conf. on New Actuators, June 1998, Bremen, Germany, pp. 499-502.

[18] Büttgenbach S. and J. Hesselbach, Shape Memory Alloy Microactuator Systems, Microrobotics and Microsystem Fabrication - Proceedings of SPIE, Vol. 3202, 1998, pp. 20-28.

[19] Kim, C.-J., A.P. Pisano, R.S. Muller and M.G. Lim, Polysilicon Microgripper, Micromechanics and MEMS: classic and seminal papers to 1990, New York: IEEE Press, 1997, pp. 203-206.

[20] Greitman G. and R.A. Buser, A Tactile Microgripper for Application in Microrobotics, Microrobotics: Components and Applications - Proceedings of SPIE, Vol. 2906, 1996, pp. 2-12.

[21] Goldfarb M. and N. Celanovic, A Flexure-based Gripper for Small-scale Manipulation, Robotica, Vol. 17, 1999, pp. 181-187.

[22] Carrazza, M.C., P. Dario, A. Menciass and A. Fenu, Manipulating Biological and Mechanical Micro-Objects Using LIGA-Microfabricated End-Effectors, Proc. 1998 IEEE Int. Conf. on Robotics and Automation, May 1998, Leuven, Belgium, pp. 1811-1816.

[23] Fischer R., D. Zühlke and J. Honkes, Gripping Technology for Automated Micro-Assembly, Microrobotics and Microsystem Fabrication - Proceedings of SPIE, Vol. 3202, 1998, pp. 12-19.

[24] Wang, Z, M.K. Jouaneh and D.A. Dornfeld, Design and Characterization of a Linear Motion Piezoelectric Micropositioner, IEEE Control Systems Magazine, February 1990, pp. 10-15.

[25] Newton, D., E. Garcia and G.C. Horner, A Linear Piezoelectric Motor, Smart Mater. Strut., 6, 1997, pp. 295-304.

[26] Holman. A.E., P.M.L.O. Scholte, W.Chr. Heerens and F. Tuinstra, Analysis of Piezo Actuators in Translation Constructions, Rev, Sci. Instrum., Vol. 66, No. 5, May 1995, pp. 3208-3215.

[27] Nelson B., S. Ralis, Y. Zhou and B. Vikramaditya, Force and Vision Feedback for Robotic Manipulation of the Microworld, Proc. 6th Int. Sym. on Experimental Robotics, 1999, pp. 433-442.

[28] Zhou, Q., P. Kallio, F. Arai, T.Fukuda and H.N. Koivo, A Model for Operating Micro Objects, 1999 International Symposium on Micromechatronics and Human Science, pp. 79-85.

[29] Zesch, W. and R.S. Fearing, Alignment of Microparts Using Force Controlled Pushing, Microrobotics and Manipulation - Proceedings of SPIE, Vol. 3519, 1998, pp. 148-156.

[30] Tanikawa, T. and T. Arai, Development of a Micro-manipulation System Having a Two-Fingered Micro-Hand, IEEE Transactions on Robotics and Automation, Vol. 15, No. 1, 1999, pp. 152-162.

[31] Nakamura T., Y. Kogure and K. Shimamura, Contact Motion Control of a Micro Operation Hand, 1999 International Symposium on Micromechatronics and Human Science, pp. 65-70.

[32] London, F. The General Theory of Molecular Forces, Trans. Faraday. Soc., 33, pp. 8-26, 1937.

[33] Hamaker, H.C. The London-van der Waals Attration Between Spherical Particles, Physica IV, No. 10, pp. 1058-1072, 1937.

[34] Israelachvili, J.N. Intermoluculer and Surface Forces, San Diego, Academic Press, 1991.

[35] French, R.H. Origins and Applications of London Dispersion Forces and Hamaker Constants in Ceramics, J. Am. Ceram. Soc., 83, pp. 2117-46, 2000.

[36] Goldfarb, M. and N. Celanovic, Modeling Piezoelectric Stack Actuators for Control of Micromanipulation, IEEE Control System Magazine, V.17, Issue 3, 1997, pp. 69-79.

[37] Spong, M.W. and M. Vidyasagar, Robot Dynamics and Control, New York: Wiley , 1989, pp. 221-237.